POLITECNICO DI TORINO

Corso di Laurea Magistrale in Ingegneria Civile

Tesi di Laurea Magistrale

A.A. 2021/2022

Experimental investigation and modelling of the compaction process in bituminous mixtures

Supervisor:

Prof. Ezio Santagata

Co-supervisors:

Prof. Davide Dalmazzo

Prof. Pier Paolo Riviera

Ing. Sadegh Yeganeh

Candidate:

José Luis E. Montoya Calle

To my parents and brother,
Thanks.

INDEX

LIST OF FIGURES

LIST OF TABLES

ABSTRACT

Compaction is a crucial topic for asphalt mixtures. In fact, the success of mix design depends on the effectiveness of compaction and its understanding is of paramount importance as part of the comparative assessment of different mixtures. Furthermore, mixtures with high compaction characteristics require lower energies to be employed during placement on site.

The main objective of this thesis was to investigate polymer-modified asphalt (PMA) mixtures – obtained by using different additives and by conveniently varying binder content and aggregate skeleton – characterized with respect to their compaction characteristics.

Several PMA samples were prepared by using three type of additives, two different binder content and two granulometric curves. The goal of this first phase was to evaluate the better combination that leads to high compaction. In the second phase, all the PMA specimens were subjected to Indirect Tensile Strength (ITS) tests. The results showed that the PMA mixtures containing the additives exhibited reduced values of ITS value due to reduction of internal friction.

In addition to the mechanical performance evaluation, the compaction characteristics were deeply analysed by means of different analytical models. These were studied and developed starting from simple models and thereafter combining them to create more complex arrangements.

The objective of this phase was to obtain a model that can simulate with high accuracy the compaction of all PMA mixtures, with the consequent identification of parameters that can highlight different aspects of the compaction phenomenon.

CHAPTER 1

Objective and outlines of the study

1.1 Introduction

The first use of asphalt materials for roadways dates to the early 1800s. From those initial tries, there have been many methodologies used for the bituminous asphalt mixture design, and the scope of each design method was to improve the material in terms of functionality and structural response.

Looking at the evolution of pavement design during past decades, the following noticeable periods can be mentioned:

- in the pre 1950s the design was based on trial and error and personal experience;
- development of empirical methods during the AASHO Road Test conducted by the American Association of State Highway and Transportation Officials;
- in the 1980s there was an initial use of Mechanical-Empirical method;
- in the 2000s there was a need to implement the Mechanical-Empirical method.

The bituminous mixtures are the material employed in the construction of flexible pavement. The flexible pavement itself present several layers, and each having specific function to be carry out, under the traffic load. These layers can be listed from the top, layer in contact with the wheels of the vehicles, to the bottom until reach the subgrade as follows:

- Surface course or waring course, this layer is removable;
- Binder course, this layer is normally included between surface course and base course;
- Base course, the layer in contact with granular material
- Sub-base course or foundation, it is composed by granular and selected material;
- Sub-grade which is the natural soil after removed the vegetation.

In the following *Figure 1* is shown an example of a typical section of flexible pavement [1].

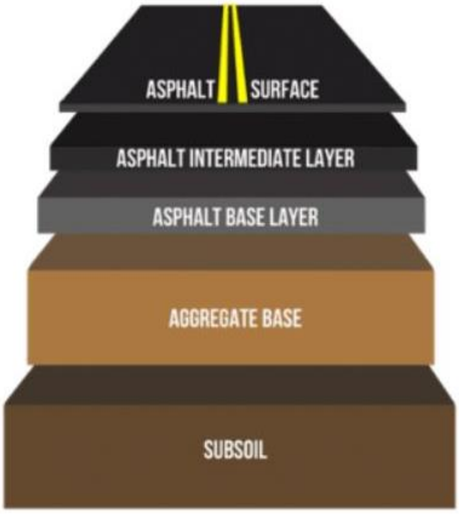

Figure 1: Typical section of flexible pavement

The focus of this study is on the binder layer, which is considered to be made by use of the polymer-modified binder (PMB).

In the last decades, road paving sectors are investing in the design of durability, sustainable and resilient infrastructures, which meet the demand deriving from economic point of view and sustainable development. In fact, one goal of many road paving sector is to improve the compaction by reducing the required effort, which can be translated into the reduction of the energy consumption.

It is known that the internal material composition of asphalt mixture reflects its characteristic; in other terms, the compaction characteristic of asphalt mixture is mainly affected by its material composition.

As mentioned, many road paving sectors are trying to improve the compaction by reducing the required effort. In this study, an Italian Company supplied the material with the aim to investigate the influence of the material composition through the compaction of asphalt mixtures varying the binder content, using different chemical additives and changing the aggregate skeleton. To this aim, the evaluation of compaction characteristics of asphalt mixture was simulated at laboratory-scale by means of the gyratory shear compactor (GSC). The GSC allowed to record the data of the variation height in function to the number of gyrations that allows to the determination of the compaction curve.

In addition, the compaction curve will be simulated by means of analytic models. The scope of using analytic models is the determination of parameters that can highlight different aspects of the compaction phenomenon.

The objective of this study and its phases are introduced in more details in next section.

1.2 Objective of the study

According to the importance of compaction in bituminous mixtures, the main objective of this study was defined based on the compaction phenomenon of the polymer-modified asphalt (PMA) mixtures, by using different additives and conveniently varying binder content and aggregate skeleton.

Based on the variable conditions considered in this study, and the lack of simple model to describe the compaction curve obtained from gyratory compactor for asphalt mixtures, an analytical model was introduced. This model is trying to express the compaction phenomena in a simple way which can be explained by basic mechanical model. The results related to the compaction and the model is completely explained in dedicated chapters.

1.3 Thesis outlines

In this paragraph is introduced the thesis outlines that allows to define this study from the beginning to the conclusions as follows:

- the first of paramount importance step of this study was to search information based on the objectives of the study, this is summarized in the CHAPTER 2: Background and Literature review;
- after collected theoretical information, the following step was the performance of the experiment, in order to collect data of the material involved in the research as the type of used material, basic and mechanical properties. This operation was performed in the CHAPTER 3: Experimental Campaign;
- at the end of the experiment follows the modelling part of the compaction curves of each type of asphalt mixtures. To do this analytical model was developed starting from simple models. This step is explained in the CHAPTER 4: Analytical Models;
- the last step of the study regards the conclusions described in the CHAPTER 5: Conclusions;

CHAPTER 2

Background and Literature review

2.1 Introduction

This chapter will describe the information collected regarding the objective of the study. In this way some theoretical notions, methods, research and so on will be introduced.

The goal of this chapter is to give to the reader the useful information, in order to understand in the followings chapters to the arguments treated.

2.2 Volumetric measurement in asphalt mixture

2.2.1 Voids in mineral aggregate (VMA)

This paragraph describes the procedure for the calculation of the VMA that is a volumetric characteristic of a compacted bituminous specimen. The voids in the mineral aggregate (VMA) are defined as volume of inter-granular void space between the aggregate particles of a compacted bituminous mixture that includes the air voids and the volume of the bituminous binder in the specimen, a schematic illustration is shown in the *Figure 2* [2].

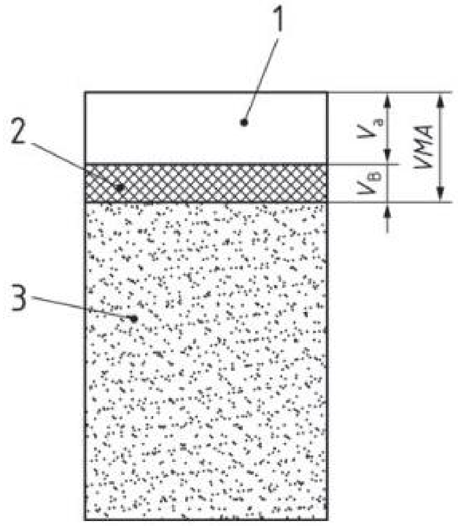

Figure 2: Voids in the mineral aggregate

where:

1 voids;

2 bitumen;

3 mineral aggregate;

VMA is calculated using the following equation, in according to the standard BS EN 12697-8:

$$\mathrm{VMA} = \frac{\rho_m - \rho_b}{\rho_m} \cdot 100 + \frac{\mathrm{B} \cdot \rho_b}{\rho_B} \tag{2.1}$$

where:

ρ_m *is the maximum density of the mixture, in megagrams per cubic metre [Mg/m^3];*

ρ_b *is the bulk density of the mixture, in megagrams per cubic metre [Mg/m^3];*

B is the percentage of the binder in the specimen (in 100 % mixture);

P_B *is the density of the binder, in megagrams per cubic metre [Mg/m^3].*

2.2.2 Void filled with asphalt (VFA)

This paragraph illustrates the procedure for the determination of the VFA that is a volumetric characteristic of a compacted bituminous specimen. The voids filled by bitumen (VFA) is defined as the percentage of the intermolecular void spaces between the aggregate particles that is occupied by effective bitumen [2].

The VFA is calculated using the following equation, in according to the standard BS EN 12697-8:

$$VFA = \frac{\mathrm{B} \cdot \rho_b \cdot 100}{\rho_B \cdot VMA} \tag{2.2}$$

where:

VMA is the voids in the mineral aggregate;

ρ_b *is the bulk density of the mixture, in megagrams per cubic metre [Mg/m^3];*

B is the percentage of the binder in the specimen (in 100 % mixture);

P_B *is the density of the binder, in megagrams per cubic metre [Mg/m^3].*

2.3 Principle of Superpave Gyratory Compactor

Among many test instruments for researching compaction characteristic of asphalt mixtures, Superpave gyratory compactor better simulate the compaction process in the field of mixtures.

In this study, Superpave gyratory compactor is used to analyse the effect of all type of material compositions on compaction characteristic using the Gyratory Shear Compactor.

Gyratory compaction moulding can simulate the action on mixtures of construction machines (rolling) and traffic load (vehicles). The main components of the Superpave gyratory compactor are [3]:

- Reaction frame, rotation and motor;
- Loading system, loading ram and pressure gauge;
- Height measuring and recording system;
- Mould and base plate.

The machine can apply a load pressure equal to 600 kPa on the sample for compaction. The SGC mould has an inner diameter of 100 mm or 150 mm. The rotation that the Superpave gyratory apply to the mould is constant at 30 revolutions per minute during compaction with the mould positioned at a compaction angle of 1.25 degrees, a schematic illustration in shown in the *Figure 3* [3].

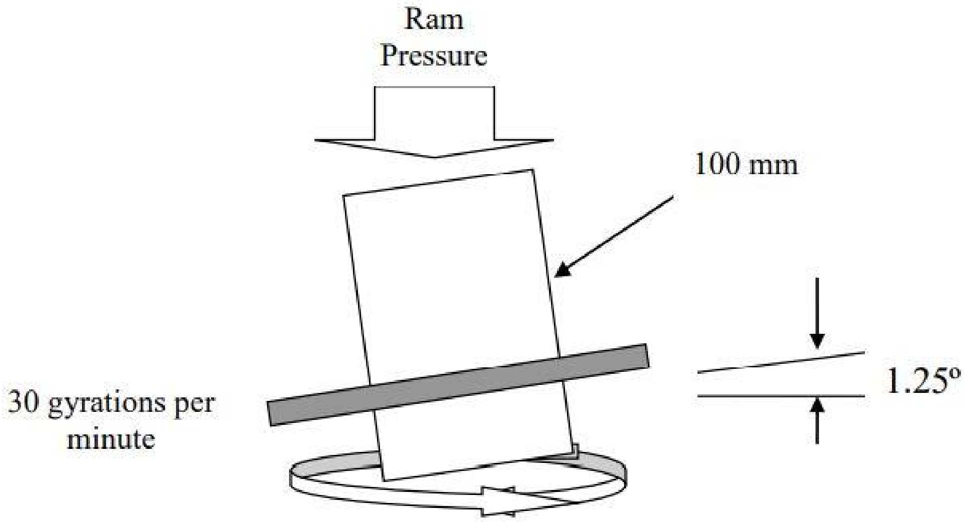

Figure 3: Schematic representation of SGC Mould and Compactive Effort

In all asphalt mix design procedures, mixtures are designed at a specific level of compaction effort. In Superpave this is a function of the design number of gyrations,

N_{des}. It is the design number of gyrations of the mixes for the determination of the asphalt content. N_{des} is function of two important variables: the traffic level (espress in ESALs) and the environmental. The standards suggest the values of the N_{des} based on the value of the ESALs. In addition to the N_{des}, there are two more gyration levels, the initial number of gyrations, N_{ini}, and the maximum number of gyrations, N_{max}. N_{ini} is the initial number of gyrations at which SGC compacted sample shall have high percent of air voids, around 11 percent. N_{max} is the maximum number of gyrations at which SGC compacted sample shall have air void more than 2 percent, in order to provide rutting [3].

2.4 Workability and Compactability

The term of "workability" is been defined to describe several properties related to the construction of hot-mix asphalt (HMA). For this study, workability was defined as a property describing the ease with which PMA can be placed, worked by hand, and compacted. This definition provides a term that is applicable to movement of PMA through equipment to the roadway, handwork of PMA, and compactability on the roadway [4].

Many indices have been reported in the literature to assess asphalt mix workability and compactability during compaction. Cabrera and Dixon (1994) determined the porosity using the air voids and number of gyration data. The intercept "a" of the porosity function with y-axis was used to evaluate the workability of the mixes. This index is referred here as Porosity Index (PI). Bahia et al. (1998) used the compaction curve data to develop two energy indices at a particular %G_{mm} related to field construction. The indices were determined using the area under the compaction curve from the intercept to 92% G_{mm} and from 92 to 96% G_{mm}. The first index (from the intercept to 92% G_{mm}) is correlated to the workability of the mix due to the volumetric change, referred herein as the Volumetric Energy Index. The second index (from 92% to 96% G_{mm}) is correlated to the shear strength of the mix due to the interlocking resistance in-between the aggregates particles; referred herein as the Shear Energy Index. These energy indices were determined by multiplying the compaction pressure, mix cross-section area, and the summation of height change. Details of these indices are presented in the *Figure 4* [5].

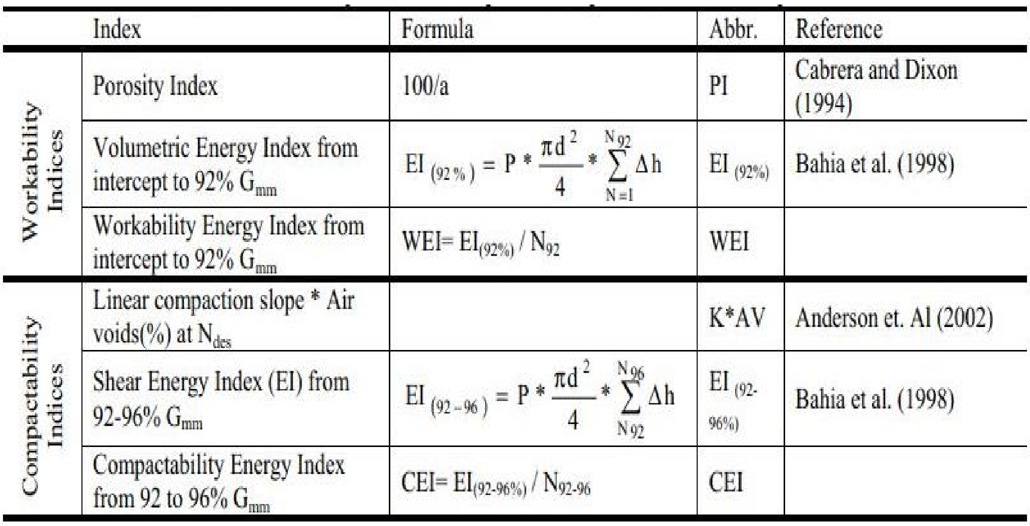

	Index	Formula	Abbr.	Reference
Workability Indices	Porosity Index	100/a	PI	Cabrera and Dixon (1994)
	Volumetric Energy Index from intercept to 92% G_{mm}	$EI_{(92\%)} = P * \frac{\pi d^2}{4} * \sum_{N=1}^{N_{92}} \Delta h$	$EI_{(92\%)}$	Bahia et al. (1998)
	Workability Energy Index from intercept to 92% G_{mm}	$WEI = EI_{(92\%)} / N_{92}$	WEI	
Compactability Indices	Linear compaction slope * Air voids(%) at N_{des}		K*AV	Anderson et. Al (2002)
	Shear Energy Index (EI) from 92-96% G_{mm}	$EI_{(92-96)} = P * \frac{\pi d^2}{4} * \sum_{N_{92}}^{N_{96}} \Delta h$	$EI_{(92\text{-}96\%)}$	Bahia et al. (1998)
	Compactability Energy Index from 92 to 96% G_{mm}	$CEI = EI_{(92\text{-}96\%)} / N_{92\text{-}96}$	CEI	

Figure 4: Summary of the Compactability and Workability indexes

2.5 Theoretical notions of simple models

The models represent the idealization of the behavior of the material under load.

In this paragraph is introducing the basic theoretical notions about simple models useful to understand the chapter of analytical models further on. In the reality simple models analysed by one by doesn’t reflect the real behaviour of the materials. Real materials under load have complex behavior and for this reason can’t be described by one simple model.

The main theories used to describe the simple models are: the elastic, the viscous and the plastic theory.

The behaviour of the models is analysed by means the creep and recovery test.

2.5.1 Linear elastic theory

The linear elastic theory is the simplest way to create a model in which the stress is linearly proportional to the strain, it consists of a spring element with stiffness modulus E, in the *Figure 5* is illustrated an example [6] [7].

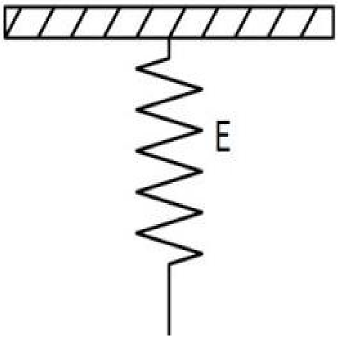

Figure 5: Spring element

The constitutive equation of the model is:

$$\sigma(t) = \mathrm{E} \cdot \varepsilon \tag{2.3}$$

From the equation (2.3), the strain to an applied load σ_0 is:

$$\varepsilon_0 = \frac{\sigma_0}{E} \tag{2.4}$$

The behavior of this element can be studied with a creep and recovery test, in the *Figure 6* and *Figure 7* are illustrated the response of the creep and recovery test.

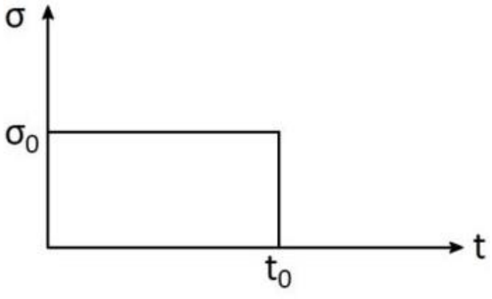

Figure 6: Creep and Recovery test of the spring - Stress

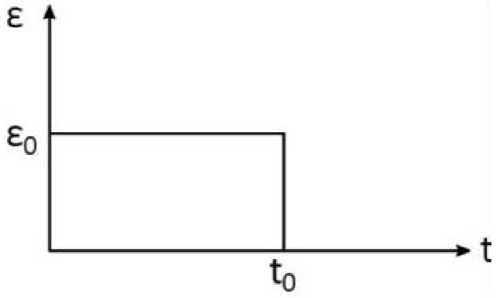

Figure 7: Creep and Recovery test of the spring - Strain

It is evident that the response of the material under load is immediately and can vary to any load change, and when the load is removed it again react instantly to the initial position.

The response of the material is obviously not very representative of the response to a real material. There is not creep stage, anelastic recovery or permanent creed strain [6] [7].

2.5.2 Linear viscous theory

Viscosity is the property of a fluid which opposes the relative motion between two surface of the fluid that are moving at different velocities. A velocity gradient is thus established and it can be verified that it is related to the applied shear by a constant η, the viscosity of the fluid, in the *Figure 8* is illustrated a schematic representation [6] [7].

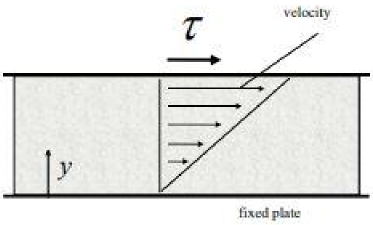

Figure 8: Schematization of Newtonian fluid

The representative equation is:

$$\frac{d\dot{v}}{dy} = \frac{1}{\eta} \cdot \tau \qquad (2.5)$$

It is possible to consider now a dash-pot, that is a piston moving in a viscous fluid of viscosity η, in the *Figure 9* the illustration of the dash-pot element.

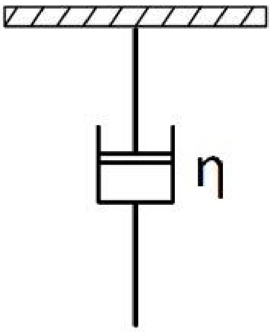

Figure 9: Dash-pot element

The equation of the dash-pot assuming the above ideal fluid behavior is:

$$\dot{\varepsilon} = \frac{1}{\eta} \cdot \sigma \tag{2.6}$$

The creep and recovery response of the material is shown in the *Figure 10* and *Figure 11*.

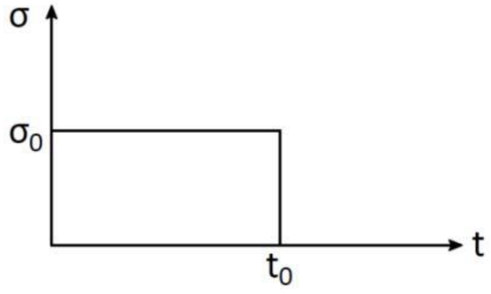

Figure 10:Creep and Recovery of the Dash-pot - Stress

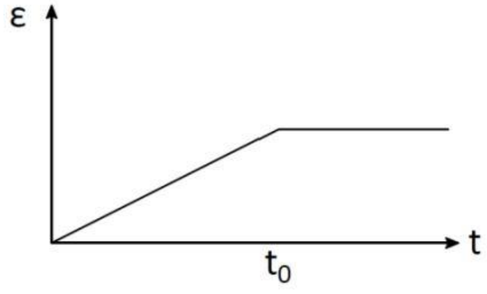

Figure 11: Creep and Recovery of the Dash-pot - Strain

In this case there is not instantaneous deformation, the slope of the creep line is σ_0/η there is a permanent strain [7].

2.5.3 Viscoelastic theory

The viscoelastic theory regards the combination of the viscous and elastic linear theories. The models developed by Maxwell and the Kelvin-Voight are considered viscoelatic models due to the combination of viscous and elastic elements.

In this section is illustrated the theory of the models developed by the two autors.

Maxwell model

The Maxwell model consists of a spring element, with elasticity modulus E, and a dash-pot, with a viscosity coefficient η, connected in series, the model is illustrated in the *Figure 12*.

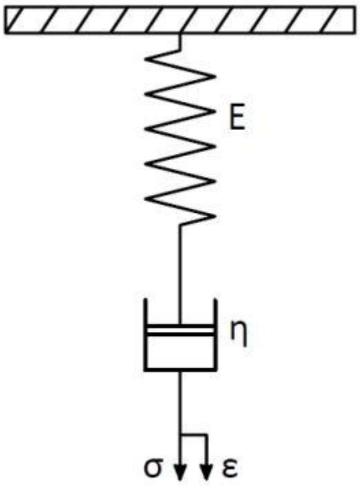

Figure 12: Maxwell model in series

In this model the stress inside both elements will be the same, while the total deformation of the model is given by the sum of the strain of the two components [6] [7].

The total deformation of the model is:

$$\varepsilon = \varepsilon_1 + \varepsilon_2 \tag{2.7}$$

Where $\varepsilon_1$is the deformation of the spring and ε_2 is the deformation of the dash-pot.

Differentiating the equation (2.7), and substituting the differentiating of ε_1 and ε_2 with their law, it is possible to evaluate the constitutive equation of the spring and the dash-pot. The constitutive equation of the Maxwell model is:

$$\sigma(\mathrm{t}) = \dot{\varepsilon} \cdot \eta - \frac{\eta}{E} \cdot \dot{\sigma} \tag{2.8}$$

The behavior of this model can be studied with the creep and recovery test, illustrated in the *Figure 13* and *Figure 14*, and the relaxation test, illustrated in the *Figure 15* and *Figure 16*.

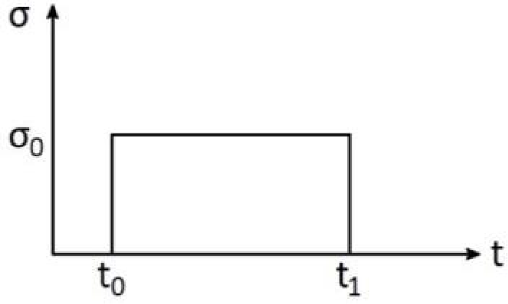

Figure 13: Creep and Recovery test of the Maxwell model - Stress

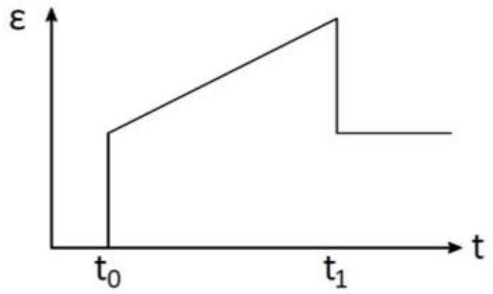

Figure 14: Creep and Recovery test of the Maxwell Model - Strain

Regarding the creep and recovery test, when the load is applied the spring stretch immediately as known, while the dash-pot acts like a rigid body; during the time in which the load is constant, the deformation of the model is increasing by the viscous element. Instead, when the load is removed the spring returns to the initial position, while the dash-pot maintains its deformation, for this combination of model at the end will remain a permanent strain caused by the dash-pot element [6] [7].

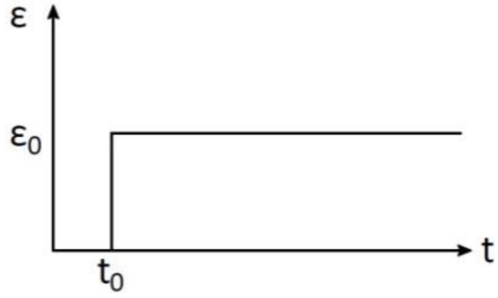

Figure 15: Relaxation test of the Maxwell model - Strain

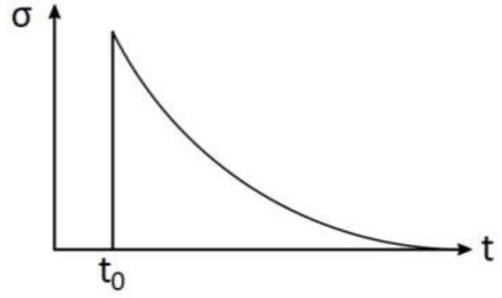

Figure 16: Relaxation test of the Maxwell model - Stress

Concerning the relaxation test, the moment when the deformation is applied the system's modulus is only the elasticity modulus of the spring, then the dashpot starts to deform while the spring contracts [6] [7].

Kelvin-Voight Model

The Kelvin-Voight model, in which consist of a spring, with elasticity modulus E, and dash-pot, with viscosity constant η, connected in parallel. In this model the strain of the spring is assumed the same to the dash-pot element, while the total stress is the sum of the ones of the two elements [6] [7].

In *Figure 17* is shown the schematization of the Kelvin-Voight model [7].

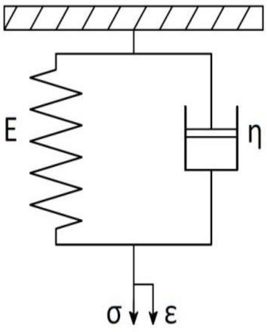

Figure 17: Kelvin-Voight model

The constitutive equation of the Kelvin-Voight model is the following:

$$\sigma(t) = E \cdot \varepsilon + \eta \cdot \dot{\varepsilon} \tag{2.9}$$

The behavior of this model can be studied with the creep and recovery test, illustrated in the *Figure 18* and *Figure 19*.

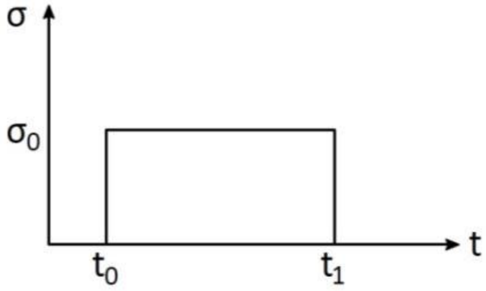

Figure 18: Creep and Recovery test of the Kelvin-Voight model - Stress

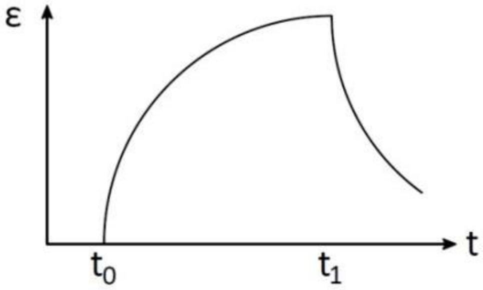

Figure 19: Creep and Recovery test of the Kelvin-Voight model - Strain

During the creep and recovery test, applying a load to the model, the spring tries to stretch immediately but is blocked by the dash-pot, which means that all the stress is taken by the viscous element. The system starts to deform with a slope depending on the viscosity of the dash-pot.

When the load is removed, the spring starts to contrast and again the dash-pot holds it back; after a given time, depending on the parameters of the model, the system will return to its initial position [6] [7].

In this model compare to the Maxwell model doesn’t react well the relaxation test, in particular, to apply the initial deformation is necessary an infinite instantaneous force [7].

2.5.4 Plastic theory

Plasticity can be considered the property of the material that can have their shape easily changed by the application of appropriately directed forces, and retain their shape upon removal of such forces [8].

It can be idealized as a slider with a certain yielding strength σ_y, the element is illustrated in the *Figure 20* [7].

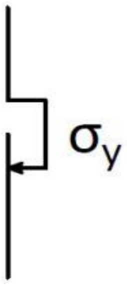

Figure 20: Slider element

its constitutive law is the follow equation:

$$\sigma(t) \le \sigma_y \tag{2.10}$$

When the load is applied, this element starts to deform only if the stress is higher than the yielding stress, and the strain continues to increase until the stress lowers, in the *Figure 21* is illustrated the diagram stress-deformation of ideal plastic behavior [7].

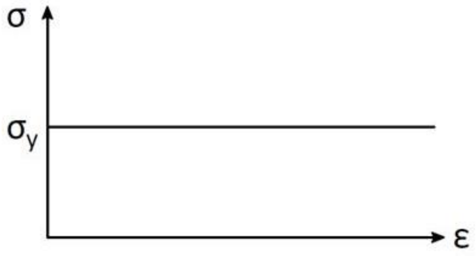

Figure 21: Plastic behavior

This result is a perfect idealization of materials, usually it is present at least a starting elastic behavior [7].

2.5.5 Elastic-Perfectly plastic theory

To improve the ideal plastic behavior, it is possible to attach a spring, with elastic modulus equal to E, to the slider, connected in series. In this way the model will have more progressive behavior.

In the *Figure 22* is illustrated the schematization of the elastic-plastic model [7].

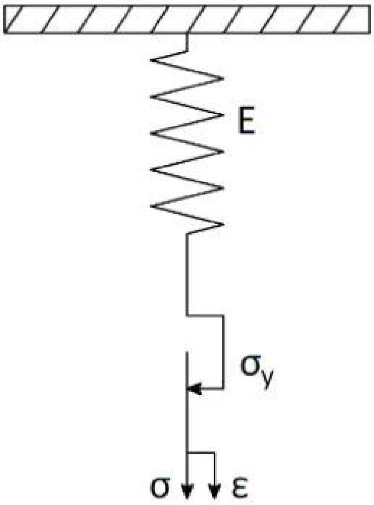

Figure 22: Elastic-plastic model

Its constitutive equation is the following:

$$\sigma(t) = E \cdot \varepsilon \leq \sigma_y \tag{2.11}$$

When the load is applied the system starts to deform with an elastic behavior until the achieving of the yielding stress, after which there is a plastic deformation and the stress inside the material is not increasing anymore, in the *Figure 23* is illustrated the diagram stress-deformation of elastic-plastic behavior [7].

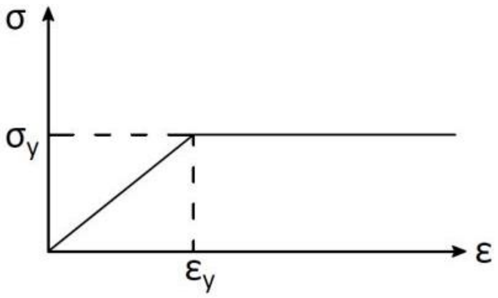

Figure 23: Elastic-plastic behavior

CHAPTER 3

Experimental campaign

3.1 Introduction

This chapter is completely dedicated to the experimental campaign. The material involved in this study was supplied by Italian Company, operating mostly in the production of chemical building materials. The request of the company for this study was to see the effect of different chemical additives in term of workability. The study is started with a bituminous mixture developed by the Company, this mean that during the experimental campaign the asphalt mixture developed by the company is used as the reference, in order to compare with the others mixtures developed in this study.

The first phase of the experimental campaign shown the material supplied by the Company, and some basic test for the determination of their basic properties. The materials involved in the experiment are:

- polymer modified binder (PMB);
- chemical additives (coded ACF-L5, ACF-EXP1 and ACF-EXP2);
- type of aggregates and filler.

The determination of the basic properties of the materials were obtained making test in the material laboratory in Politecnico di Torino. This first step is of paramount important, due to the fact that the knowledge of the characteristic of the material by the basic properties given idea of their behavior and permit to classify them.

In the second phase of the experimental campaign are illustrated the testing that allows to the creation of the specimens by the Gyratory Shear Compactor (GSC). The compaction is the process by which the asphalt and aggregate are compressed into a reduced volume. In this step is shown the first goal of the study, several compaction tests were performed, in order to evidence the difference of compactions effort of the mixtures using different chemical additives and conventionally varying the binder content and the aggregate skeleton.

The last phase of the experimental campaign was the determination of the mechanical properties of the samples created by the compaction test. The Indirect Tensile Strength (ITS) was the test selected to put in evidence the mechanical properties of the obtained samples. The advantage of the ITS test are the simplicity and the rapidity.

All the test were performed from the laboratory test of the Politecnico di Torino (D.I.A.T.I.).

3.2 Materials and Basic properties

3.2.1 Polymer modified bitumen (PMB)

In the present study, polymer modified bitumen (PMB) was used as bitumen in the asphalt mixture. The company supplied with many containers of about 5kg each, show in *Figure 24*. The PMB inside of the containers of 5 kg were heated and poured out into small containers in which the capacity was enough for one mixture, illustrated in *Figure 25*. Before poured out the small containers the PMB was mixed inside its container.

Figure 24: container with PMB, capacity 5 kg

Figure 25: Containers with PMB, capacity 250 ml

In the following *Table 1* is illustrated some properties of the binder. The values of the needle penetration and the softening point were tested by the Company [9], and dynamic viscosity was evaluated in the laboratory of the Politecnico di Torino using the Dynamic Shear Rheometer (DSR).

Table 1: Properties of the PBM

Test	Standard	T. [°C]	Result
needle penetration	EN 1426	25	62 dmm
softening point	EN 1427	5 [1/min]	78 °C
dynamic viscosity	EN 13302	165	0.451 Pa·s

3.2.2 Chemical additives

The chemical additives supplied by the Company for this experimental campaign are three types: ACF-L5, ACF-EXP1 and ACF-EXP2. The first one (ACF-L5) is found in the commercial market and it is sold as high-performance regenerating liquid admixture, instead, the others two are experimental additives.

In the *Figure 26* is illustrated a picture of the chemical additives.

Figure 26: Chemical additives

The three additives supplied are synthetic liquid, their special formulation should improve the compaction of bituminous mixture reducing the compaction effort.

The characteristic of the additives, especially for the ACF-L5 is shown in the *Table 2* [10].

Table 2: Characteristic of the additives

Additive	Consistency	Colour	Density
ACF-L5	liquid	clear yellow	0.92 ± 0.02 [g/cm^3]
ACF-EXP1	liquid	dark brown	-
ACF-EXP2	liquid	dark yellow	-

The additives were added, in 2% of the relative weight of the binder, and mixed directly into the bitumen at 150 °C.

In *Figure 27* is shown the heater used to keep the temperature of the binder at 150 °C. On the top of the heater was added, as shown, a cover in metal with a hole to put inside the container of binder, in order to keep uniform the temperature from the bottom to the top of the container. Regarding the mixing part, it was made through the overhead stirrer, as shown in *Figure 28*, for at least 4-5 minutes.

Figure 27: Heater for small containers, capacity 250 ml

Figure 28: Overhead stirrer, Heidolph type RZR

This kind of procedure was used to mix all the three additives with the binder and every time was made during the preparation of the bituminous conglomerate. Every time the additives were added to the binder only in the preparation of the asphalt mixture, in order to do not lose the effect of the additives during the time.

In conclusion, in *Table 3* is shown the information regarding the dynamic viscosity property of the PMB with the additives. It was tested using the DSR as the binder was tested.

Table 3:Values of the dynamic viscosity of the binder with and without additives

Bitumen	Test	Standard	T. [°C]	Result
PMB	dynamic viscosity	EN 13302	165	0.451 [Pa·s]
PMB+ACF-L5 (2%)	dynamic viscosity	EN 13302	165	0.356 [Pa·s]
PMB+ACF-EXP1 (2%)	dynamic viscosity	EN 13302	165	0.358 [Pa·s]
PMB+ACF-EXP2 (2%)	dynamic viscosity	EN 13302	165	0.375 [Pa·s]

3.2.3 Aggregate

Aggregates includes the majority of the material used in asphalt mixture, in a typical asphalt mixture, aggregate can represent up to around 95 % of the total weight. They serve various functionalities for the asphalt pavement, one of them is the load-supporting.

The material stocked by the Company consisted in four different particle size classes, in *Figure 29* is illustrated the different class of aggregates:

- fine sand (dimension from 0 to 4 mm);

- coarse sand (dimension from 2 to 6 mm);
- crushed stone (dimension from 6 to 12 mm);
- crushed stone (dimension from 10 to 20 mm).

Figure 29: Aggregate size class

Since each aggregate size class present a collection of aggregate, one of the most important characteristic, it is to look the aggregate gradation, called also particle size distribution.

In this section is illustrated the particle size distribution and particle density. The particle density describes the physical properties of the material.

Particle size distribution

The particle size distribution has been evaluated with the sieving method, according to BS EN 933-1:2012 [11].

The selection of the sample for the evaluation of the particle size distribution has been obtained by quartering, in *Figure 30* is shown an example of quartering, according to the standard BS EN 932-2:1999 [12].

Figure 30: Quartering the material

The minimum test portion mass was calculated using the following formulae:

$$M = \left(\frac{D}{10}\right)^2 \tag{3.1}$$

where:

M = minimum mass of the test portion, in kilograms [kg];

D = aggregate size, in millimeters [mm].

Defined the representative sample, before start the test it has been dried using an oven at temperature of 105 ± 5 °C, according to the BS EN 933-1:2012 [11], after dried, the mass of the initial sample was recorded (M_1).

The following step has been washed the sample using two sieves, the sieves 2 mm and 0.063 mm assembled in column. The first process was poured and washed the material inside of the sieve 2 mm, after washed the retained 2 mm, the second process was to remove the sieve 2 mm and washed the retained 0.063 mm until the water was clear. The washing process was performed carefully, in order to do not lose any aggregate during the process. At the end of the washing before record the mass of the washed material (M_2), it was necessary dried the washed material to remove the remained water. In this way, it was possible define the mass of the passing 0.063 mm computing the difference between mass M_2 and M_1. This operation of paramount important, in order to have better results after the sieve shaking, because the filler could remain attached in the surface of the aggregates, overestimating the weight of the retained material inside each sieve.

Before starting the shaking test to the washed sample, a column of the required sieves has made, in which the aperture size is decreasing from top to the bottom. In this step is important record the weight of each sieve, in *Figure 31* is shown the column of the required sieves.

Figure 31: Column of sieves required

In this study were used UNI sieves, which openings, in mm, are: 20, 16, 14, 12.5, 10, 8, 6.3, 4, 2, 1, 0.5, 0.25, 0.125, 0.063.

One time the sieve column is assembled, the aggregates are located at the top of the sieves pile. In this way the sieve column was placed on the sieve shaker, shown in *Figure 32*, after fix the sieve column to the sieve shaker is activated by electromagnetic impulses and has a triple vibrating action (vertical, lateral and rotational); the vibration continues for 10 minutes.

Figure 32: Seave shaker

At the end of the test, each sieve is weighed to measure the retained material for each opening; knowing the weight of each sieve, the weight of the sieve with the retained material and the initial total weight is possible to obtain the progressive passing and build the particle size distribution curves.

The equations used are:

- partial retained [%]:

$$r_i = 100 \cdot \frac{m_i}{m_{tot}} \tag{3.2}$$

- progressive retained [%]:

$$R_i = \sum_{j=0}^{i} r_j \tag{3.3}$$

- progressive passing [%]:

$$r_i = 100 - R_i \tag{3.4}$$

For each granular size class, it is been performed two tests in order to avoid doubts with the material.

In the following *Graph 1* is shown the average of the test for each particle size distribution curve.

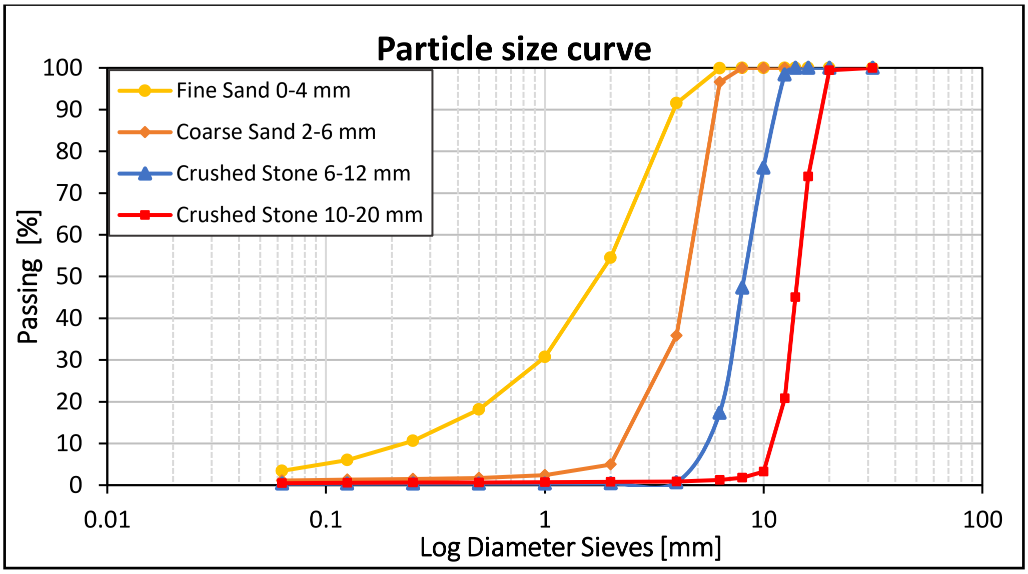

Graph 1: Distribution curve of the aggregate

Particle density

The physical properties of the aggregate are the particle density evaluated through the pycnometer method, according to the standard BS EN 1097-6: 2013 [13].

As in the particle size distribution, the sample was selected in according to the BS EN 932-2 by quartering [12] . Instead, the minimum mass of the test portion for each particle size class is reported in the standard, that is depending from the maximum aggregate size for each class [13]. Before to start the test, the material was dried in the oven at 105 ± 5 °C, in order to remove the humidity.

The procedure to obtain the particle density is shown in the following steps in according to the standard [13]:

- the test begun weighing the empty pycnometer with its corresponding head (M_0) and the pycnometer with the testing sample (M_1), shown in *Figure 33* and *34*;

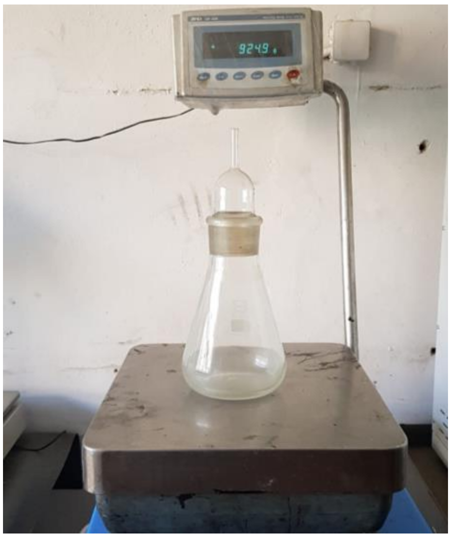

Figure 33: Weighing empty pycnometer

Figure 34: Weighing pycnometer with the sample

- then it was poured inside the pycnometer distilled water and carefully stirred with a glass rod to remove the entrapped air and adherent air bubble, the result of the stirred is shown in the *Figure 35*;

Figure 35: Result after stirred the material inside the pycnometer

- After stirred, the pycnometer was left until the water appeared clean, the waiting time is increasing as the granular size class is decreasing, then the remained entrapped air was removed by applying a vacuum for at least half an hour, shown in *Figure 36* and *37*.

Figure 36: Vacuum system

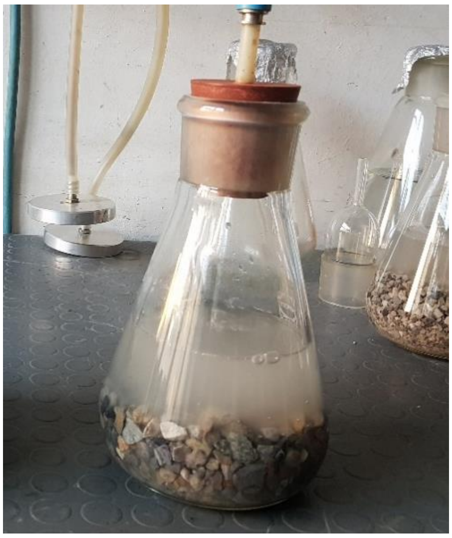

Figure 37: Performing the vacuum

- After the vacuum refilled the pycnometer and its head with distillate and de-aired water, then it was recorded the weight (M_2) and the test temperature, *Figure 38* and *39*.

Figure 38: Weighing pycnometer with the material and water

Figure 39: Recording the test temperature

Knowing the required mass, the particle density is calculated according to the following equation:

$$\rho_p = \frac{M_1 - M_0}{V - \frac{(M_2 - M_1)}{\rho_w}} \tag{3.5}$$

where:

M_0 is the mass of the pycnometer and funnel, in grams [g];

M_1 is the mass of the pycnometer, funnel and material, in grams [g];

M_2 is the mass of the pycnometer. funnel, material and water, in grams [g];

P_w is the density of the water, in megagrams per cubic meter [Mg/m3];

V is the volume of the pycnometer, in millimitres [ml].

In the *Table 4* is showed the results of the particle density for each particle size class.

Table 4: Particle density of the aggregate

Aggregate class	**Standard**	**Density**
Fine sand 0/4	EN 1097-6	2.797 [g/cm^3]
Coarse sand 2/6	EN 1097-6	2.771 [g/cm^3]
Crushed stone 6/12	EN 1097-6	2.705 [g/cm^3]
Crushed stone 10/20	EN 1097-6	2.721 [g/cm^3]

3.2.4 Filler

In addition to the aggregate, the company supplied the filler, that play a significant role on the performance of asphalt mixture, the *Figure 40* is illustrated the filler used in this study.

Figure 40: Filler, passing 0.063 mm

In the same way of the aggregates, the particle size distribution was performed using the sieving method. The result of the test is shown in the *Graph 2*.

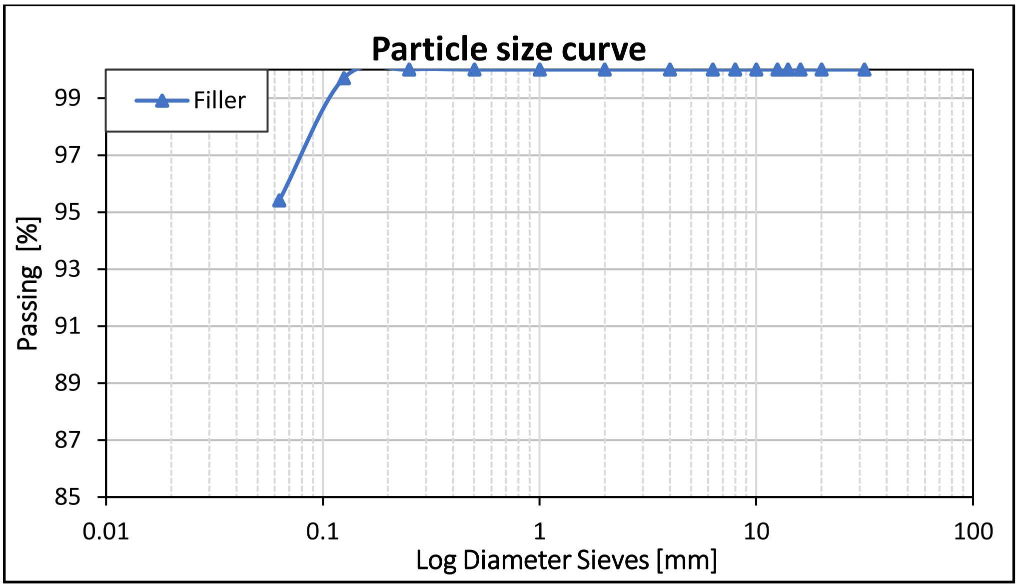

Graph 2: Distribution curve of the filler

Regarding the particle density for the filler the test was performed according to the standard BS EN 1097-7: 2008 [14]. The test result is shown in the *Table 5*.

Table 5: Particle density of the filler

Material	**Standard**	**Density**
Filler	EN 1097-7	2.700 [g/cm^3]

3.3 Bituminous mixture

Bituminous mixtures or asphalt mixtures are blended with different gradations of aggregates, filler and content bitumen of different grades and quantities, in the *Figure 41* is illustrated the material involved in the bituminous mixture.

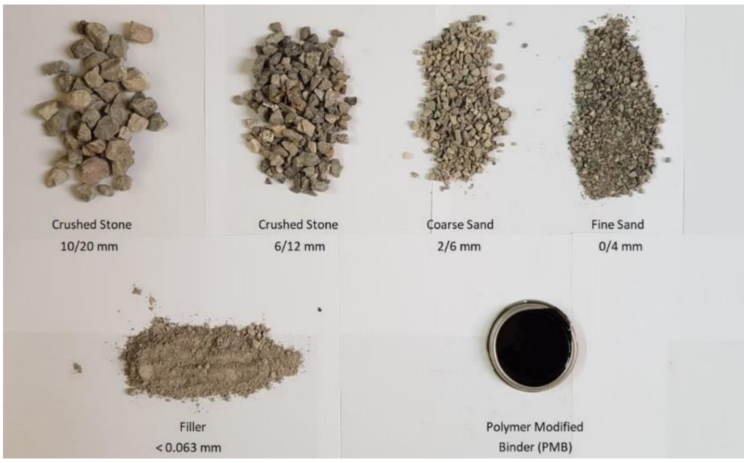

Figure 41: Aggregates, filler and bitumen

As known exist different types of bituminous material designed and in this experiment is treated the binder layer. Remembering, the binder layer is known mostly as the layer between the surface layer, the layer in contact with the vehicle, and the base layer, the layer in contact with the subgrade.

In this section is illustrated the phases from the design of the granulometric skeleton and binder content to the control of the production of the bituminous mixture. The initial phases that come before the production of the mixture are the design of the granulometric skeleton and design of the binder content. Once the skeleton and the binder content are defined the following step is the production of the bituminous mixture mixing all the material together. After the mix production is important the determination of its physical properties called theoretical maximum density and the control of the mix design through checking test of binder content and the granulometric curve.

3.3.1 Granulometric design curve

The granulometric distribution curve of asphalt mixture is the most characteristic that allows to identify the type of asphalt mixture and type of asphalt pavement.

In this study the granulometric design curve is defined using guide of the Italian standard (Capitolato Speciale di Appalto – CSA) that provides the lower and upper limits of the design curve. In the following *Figure 42* is shown the limits of the design curve from the CSA [15].

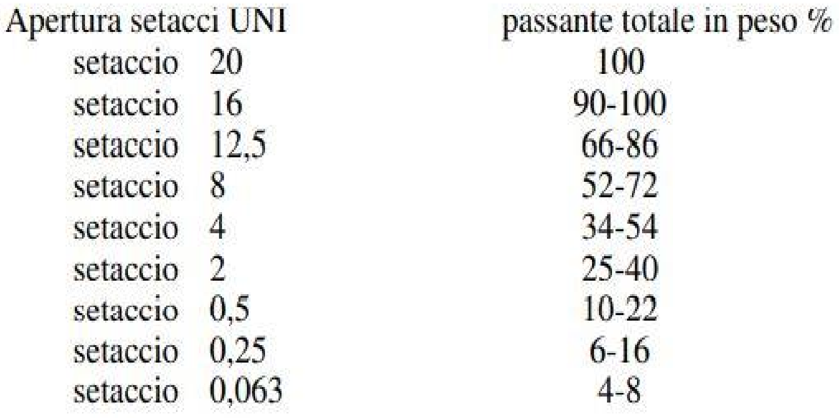

Apertura setacci UNI		passante totale in peso %
setaccio	20	100
setaccio	16	90-100
setaccio	12,5	66-86
setaccio	8	52-72
setaccio	4	34-54
setaccio	2	25-40
setaccio	0,5	10-22
setaccio	0,25	6-16
setaccio	0,063	4-8

Figure 42: Upper and lower limits from CSA

The upper and lower limits given the boundaries of the possible design curve. In other terms the design curve is the curve that remain inside the limits impose by the CSA, otherwise, it is not acceptable.

For this experimental campaign two kind of design curve were studied. One curve design was the one from the Company, the code of this granulometric skeleton is A. The second curve design were obtained using as reference the curve in the middle between the limits. To do this a optimization algorithm was used. Through the solver of "excel", the granulometric design curve was computed trying to minimize the difference between the design curve and the reference one, in the following is shown the formulae used.

$$\sum_{i=1}^{n} (P_{des}^{i} - P_{opt}^{i})^2 = \min \tag{3.6}$$

Where:

P_{des}^{i} = *passing centre limit curve at sieve i, in percentage [%];*

P_{opt}^{i} = *passing optimize at sieve i, in percentage* [%].

At the end of the process the given result is the curve with the minimum detachment from the passing centre limit curve, instead the code of this granulometric skeleton is B.

In the following *Table 6* is illustrated the passing of the two granulometric curve design used.

Table 6: Granulometric design curve

Sieves UNI	Lower Limit	Upper Limit	Centre Limit	A Design	B Design
20	100	100	100	100	100
16	90	100	95	95	93
12.5	66	86	76	83	78
8	57	72	62	71	61
4	34	54	44	51	46
2	25	40	32.5	30	30
0.500	10	22	16	14	15
0.250	6	16	11	11	11
0.063	4	8	6	8	8

In order to see better the granulometric design curve used, in the following *Graph 3* and *4* are shown the trend of the curves compare to the centre limit curve.

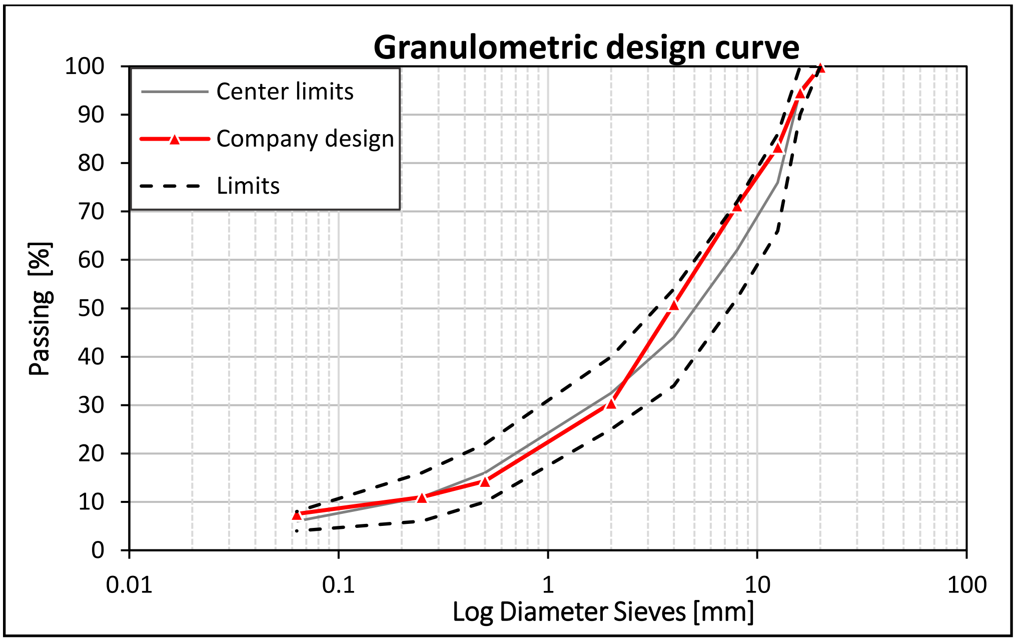

Graph 3: Granulometric design of A

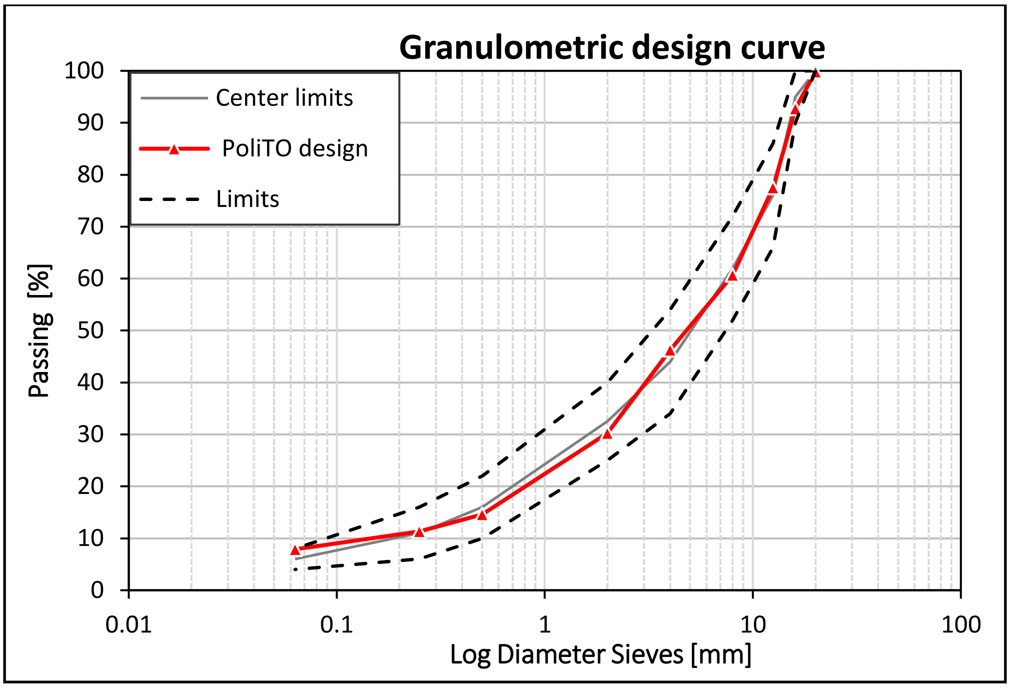

Graph 4: Granulometric design of B

Checking the results of the two granulometric design curves, both are respecting the limits, but comparing the two curves it is been evident that in term of uniformity the B curve has better gradation of aggregates than the A curve. In others words, referring to the compaction it is expected that the B curve will be more compacted due to the less space between particles.

Furthermore, using the B design curve, the aggregate size class 2/6 mm is not necessary.

In the next *Table 7* is summarize the percentage used for each aggregate size class including the filler, in order to determinate the quantity to the respective design curve.

Table 7: Percentage necessary to form the granulometric design curve

Material	G1 design	G2 design
Fine sand 0/4	43.2 %	43.0 %
Coarse sand 2/6	14.1 %	0.0%
Crushed stone 6/12	16.0 %	22.6 %
Crushed stone 10/20	20.7 %	27.9 %
Filler	6.0 %	6.5 %

3.3.2 Design binder content

Asphalt binder content as the aggregate play an important role in the HMA mixture performance. For examples excessive binder content leads to rutting, bleeding and wash boarding, in the others hand lower binder content will lead to fatigue cracking. Binder content is a sensitive parameter and it affects the volumetric properties of the bituminous mixture [16].

Regarding the binder content the CSA provides the recommended range for the binder layer, shown in the *Figure 43* [15].

4,1%-5,5% (UNI EN 12697-1 e 39)

Figure 43: Range of binder content from CSA

In the current study two type of percentage were used, one suggested by the Company and the second one it was selected to see the effect of the increasing binder in term of compaction, the percentage used are shown in the *Table 8*. The percentage of binder is based on the weight of the mixture.

Table 8: Binder content used

Binder content
4.5 %
4.9 %

3.3.3 Laboratory mixing

The process for the production of the bituminous mixture is called mixing phase, the procedure to the mixture production is in according to the standard BS EN 12697-35:2016 [17] .

In this study the mixing has been performed by hand, using a heater with low capacity (maximum 5 Kg), in *Figure 44* is illustrated the mixer used to the production of the mixtures.

Figure 44: Mixer for the production of the bituminous mixture

Before the mixing begins, it is of paramount important the preparation of the material. In this phase, it is necessary to have the right weight of the aggregate and filler. Regarding the weight of the binder should be more than the necessary, due to the fact that some portion of the binder remain stuck in the container walls. In the following *Figure 45* is shown an example of the material prepared for the mixing process.

Figure 45: example of material prepared for the compaction process

Once the material was prepared, the following step is the heating of the materials inside an oven at the mixing temperature. In this study the mixing temperature is 160 °C.

In the case of mixing with the additives as mentioned before in the previous paragraph, the additives were added to the polymer modified binder during the heating phase of the material before the mixing phase.

Once reached the desire temperature, the mixing has been performed following the steps:

- taken out from the oven the mixer bowl with the aggregate, then put it inside the heater and started the mixing process of the aggregate for 1 minutes using a spatula, *Figure 46*;

Figure 46: mixing the aggregates

- after mixed the aggregate for 1 minutes put the bowl on the balance, set zero, and poured the mixing bowl with at least half of the required binder, shown in *Figure 47*, then put back the bowl inside the heater and mixed again for 1 minutes, shown in *Figure 48*;

Figure 47: Pouring the binder

Figure 48: Mixing the poured binder

- again after 1 minutes of mixing the aggregate with the binder it was added half of the required filler and mixed for at least 30 second, shown in *Figure 49*;

Figure 49: Pouring half of the required filler

- then it was put again the bowl on the balance, set zero, and poured the mixer bowl with the left binder quantity that needs to have the binder content target, then put back the mixer bowl inside the heater, and mixed for 1 minute, shown in *Figure 50* and *51*;

Figure 50: Pouring with the left required binder

Figure 51: Mixing the poured binder

- as last was added the second half of the left filler and mixed for at least 30 second, shown in *Figure 52*.

Figure 52: Pouring the left filler

- the mixing phase is finished as all the aggregates and filler are completely cover with the binder, usually the mixing process is finished after 5-6 minutes.

The mixing process is the same for each bituminous mixture produced during this experiment campaign.

One important consideration, during the mixing process of the binder with the additive has been easier than without. In particular, the additive ACF-L5 and ACF-X1 covered easily all the aggregates. It can be translated that for these types of mixtures the workability in the mixing process increase, reducing the mixing effort.

Once the mixing is completed follows directly the compaction and the calculation of the theoretical maximum density (TMD). Before to go in the compaction process, in the next section is illustrated the test of the TMD.

3.3.4 Nomenclature of the bituminous mixtures

In this paragraph is introduced a nomenclature necessary to make clear the nominations of the bituminous mixtures performed during the experimental campaign.

g/b/a/t

Where:

g= A or B, represent the aggregate skeleton;

b= binder content in the weight of the mixture, in percentage;

a= X, Y or Z, where ACF-L5=X, ACF-EXP1=Y and ACF-EXP2=Z;

t= compaction temperature, in °C.

3.3.5 Theoretical maximum density

The theoretical maximum density (TMD) is fundamental physical properties whose values are influenced by the composition of the mixture, in terms of types and amounts of aggregates, asphalt binder content, and other materials present in the mixtures.

The TMD of the conglomerate bituminous is consider as the voidless mass. The determination of the theoretical maximum density consists into volumetric procedure with the pycnometer method, according to the standard BS EN 12697-5: 2018 [18].

The first step in the procedure was the preparation of the sample, separating the mixture into coarse particles and agglomerations, as shown in the *Figure 53*. The crucial part has been the agglomerations which should not have been larger than 6 mm, otherwise the result is not representing the sample [18].

Figure 53: Mixture into coarse particles and agglomerations

Once the sample is prepared the volumetric calculation of the TMD is performed in the following procedure, according to the standard [18]:

- The first step is weighed the empty pycnometer (m_1), shown in *Figure 54*, then weigh the pycnometer with the sample (m_2), shown in *Figure 55.* The volume (V_p) of the pycnometer is known;

Figure 54: Weighing empty pycnometer

Figure 55: weighing the pycnometer with the sample

- Then poured the pycnometer with distilled water and evacuated the entrapped air by applying a partial vacuum that results in a residual pressure of 4 kPa or less for at least half an hour, shown in *Figure 56*;

Figure 56: Applying the vacuum

- after the vacuum, refilled the pycnometer with distillate and de-aired water, recorded the weight (m_3) and the test temperature, as shown in *Figure 57* and *58*.

Figure 57: Weighing the pycnometer with the material and de-aired water

Figure 58: Recording the testing temperature

Once all the required mass are obtained, the theoretical maximum density is calculated using the following equation [18]:

$$\rho_{mv} = \frac{m_2 - m_1}{10^6 \cdot V_p - \frac{(m_3 - m_2)}{\rho_w}} \tag{3.7}$$

where:

m_1 is the mass of the pycnometer and head, in grams [g];

m_2 is the mass of the pycnometer, head and test material, in grams [g];

m_3 is the mass of the pycnometer, head, test material and water, in grams [g];

P_w is the density of the water, in megagrams per cubic meter [Mg/m^3];

V_p is the volume of the pycnometer, in cubic meter [m^3].

In the *Table 9* is showed the average of the theoretical maximum density of each type of bituminous mixture produced in this experimental campaign.

Table 9: Results of the TMD

Sample	TMD [g/cm^3]
A/4.5/160	2.552
A/4.5/X/160	2.552
A/4.5/Y/160	2.552
A1/4.5/Z/160	2.552
A/4.9/160	2.540
A/4.9/Y/160	2.540
B/4.5/160	2.557
B/4.5/Y/160	2.557

3.3.6 Control binder content

In this step is illustrated the test method for the control of the binder content of the bituminous mixtures. For the determination of the binder content was used a specific oven (carbolite) that can reach high temperature, in order to burn the binder inside the asphalt mixture. This test was performed according to the standard BS EN 12697-39: 2020 [19].

In the following *Figure 59* is illustrated the oven used for burn the binder, the temperature that the oven work is 540 °C.

Figure 59: Oven for burn the binder

Before to begin the test, the preparation of the sample is important, in order to have coarse particle and agglomerations. Regarding the sample mass, the standard suggested the minimum mass for the evaluation of the test [19].

The percentage of binder content in the mixture has been calculated following the steps:

- The first step is weighed the empty metal basket (m_1), shown in *Figure 60*, and poured the basket with the material, the sample was uniformly dispersed on the two surfaces of the basket, shown in *Figure 61*;

Figure 60: Weighing the empty basket

Figure 61: The sample inside the basket

- Then it was placed the basket inside the carbolite at 540 °C, and started the test, the waiting time was at least half an hour, shown in *Figure 62*.

Figure 62: Basket placed inside the Carbolite

- Once the test is finished it was taken out the basket, and left it cool in safety as shown in *Figure 63* and measured the weight (m_3).

Figure 63: Material getting cold in safety

Knowing all the required mass, the binder content is calculated using the following formulae:

$$\%\mathrm{B} = \frac{m_3 - m_1}{m_2 - m_1} \cdot 100 \tag{3.8}$$

where:

m_1 is the mass of the basket, in grams [g];

m_2 is the mass of the basket and test material, in grams [g];

m_3 is the mass basket and the material after ignition, in grams [g];

The results of the test performed during the experiment are reported in the *Table 10.*

Table 10: Results of the control of binder content

Sample	**Binder content design**	**%B**
A/4.5/160	4.5 %	4.43 %
A/4.5/X/160	4.5 %	4.47 %
A/4.5/Y/160	4.9 %	4.85 %

As shown the results are consistent with the binder content design.

3.3.7 Control particle size distribution

The sample used for the control of the particle size distribution has been the remained material obtained at the end of the binder content test by ignition.

In this experimental campaign this test was performed only for the bituminous mixture using the aggregate skeleton suggested by the Company.

The procedure to obtain the particle size distribution is the same used in the paragraph 3.2.3, according to the standard BS EN 933-1:2012 [11].

The result of the test is shown in the *Graph 5*, it shown the result of the distribution curve design and the control distribution curve, in order to see the difference of the two curves.

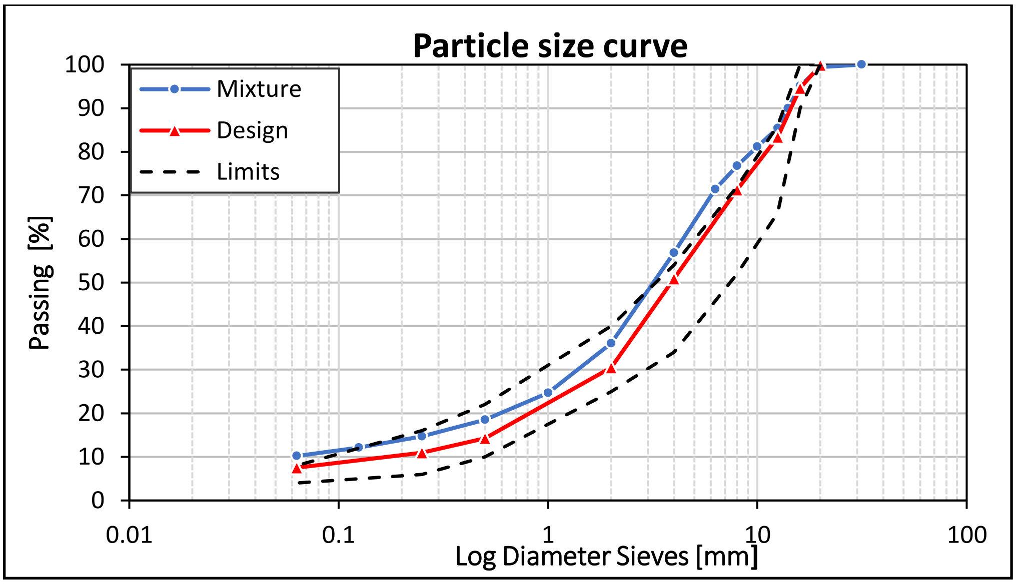

Graph 5: Control of the distribution curve

From the *Graph 5* is evident a translation of the control distribution curve to the left side compare to the design Company curve. Furthermore, the fraction 4/12.5 mm is overpassing the upper limit. In base to the results, the granulometric skeleton of the bituminous mixture resulted finer than the distribution curve design.

3.4 Volumetric analysis by GSC

Nowadays the way to understand the compaction phenomena of asphalt mixture is using the Gyratory Shear Compactor (GSC). The importance of use the GSC, due to the fact that it better simulates the real compaction in the field through the action of the steamrollers during the construction phase.

In the compaction process the variation of the volume of the specimen inside the mould is continuously measured as function of the gyration. Through this measure data and the characteristic of the final specimen are been possible the reconstruction and evaluation of the follow parameters:

- Compaction variation (%C);
- Voids in mineral aggregate (%VMA);
- Voids filled with asphalt (%VFA).

The results of the parameters are reported in the follows paragraphs, in which it is explain the procedure to obtain them.

3.4.1 Compaction curve (%C)

In this study the compaction process was obtained in according to the standard BS EN 12697-31: 2019 [20].

In the following *Figure 64* is shown the Gyratory Shear Compactor used in this experimental campaign.

Figure 64: GSC machine

The machine used can work in function of the number of gyrations and in function of the final height of the sample. In this experiment each sample has been obtained in function of the gyrations.

As mention in the paragraph 2.3 the compaction is achieved by the simultaneous action of static compression load equal to 600 kPa, and of the shearing action. In order to activate the shearing motion, the mould has an inclination angle of 1.25° generating a conical revolution surface, in this way the combination of the static force and the inclination angle allows to reach a realistic compaction, with a continuous rearrangement of the particles. Furthermore, to complete the equipment of the GSC in *Figure 65* is shown: the cylindrical mould with inner diameter of 100 millimetre, the bottom plate, the top plate and the filters.

Figure 65: Mould, plates and filters

The sample mass used for each compaction was suggested by the Company and it was around 1305 grams.

Regarding the compaction temperature, in the following *Table 11* is shown the temperatures used for the compaction of the specimens.

Table 11: Compaction temperatures

Temperature
160 °C
140 °C
110 °C

Now, following the operation below it is possible to create the samples through the compaction process, according to the standard [20]:

- First of all, it was placed the moulds and the inserts for at least two hours inside the oven to the reference compaction temperature, shown in *Figure 66*;

Figure 66: Heating the moulds

- Then the moulds were taken out and poured the with the material at the compaction temperature. The moulds were poured all at the same time, in order to have more homogeneous material inside each mould, in the *Figure 67* and *68* are shown the process;

Figure 67: Pouring the mixture inside the moulds

Figure 68: Weighing the poured material

- After poured the moulds, put back inside the oven the moulds with the material and measured the temperature of the mixture in the centre of the moulds, this operation taken at least half an hour to reach again the compaction temperature;
- When the temperature reached the compaction temperature, taken out the mould and it is inserted inside the GSC, shown in the *Figure 69*, then closed the door and started the test;

Figure 69: Mould ready for the compaction

- the test finished after 200 rotations, at a constant speed of 30 rpm, then the sample is extruded, shown in *Figure 70* and *71*.

Figure 70: Mould placed for the extraction

Figure 71: Extraction of the sample

As known the machine can record the height of the sample at each round, from this data is possible to calculate the volume and its geometrical density that leads to the determination of the geometrical compaction curve.

Since the geometrical compaction curve is not representing the real compaction curve of the material, it was necessary correct the geometrical density using a correction factor, in order to determinate the corrected density at each round, the following equation shown the correction factor:

$$C.F. = \frac{\rho_{real}}{\rho_{geometrical}} \tag{3.9}$$

Where:

ρ_{real} *is the bulk density of the sample, in grams per cubic centimetre [g/cm^3];*

$\rho_{geometrical}$ *is the geometrical density of the sample, in grams per cubic centimetre [g/cm^3].*

Before to calculate the correction factor, it was necessary the determination of the bulk density. The procedure to do this is illustrated below.

Bulk Density

The test method used to the determination of the bulk density has been the saturated surface dry (SSD) in according to the standard BS EN 12697-6: 2020 [21].

The test was carried out as follows:

- the first step id recorded the mass of the dried specimen (m_1), shown in *Figure 72*;

Figure 72: Weighing the dried sample

- then the sample was immersed in the water-bath, in order to saturate the specimen, this process required at least half an hour, shown in *Figure 73*;

Figure 73: Sample immersed in the water-bath

- once the sample is saturated, it was recorded the mass of the sample immersed in the water (m_2), shown in *Figure 74*;

Figure 74: Weighing the saturated sample immersed in water

- then the sample was removed from the water-bath and dried the surface from adhered drops by wiping with a damp Chamois, shown in *Figure 75*;

Figure 75: Drying the surface of the saturated sample

- At the end recorded in the air the mass (m_3) of the saturated and surface wiped sample, shown in *Figure 76*, and measured the temperature of the water, shown in *Figure 77*;

Figure 76: Weighing saturated sample

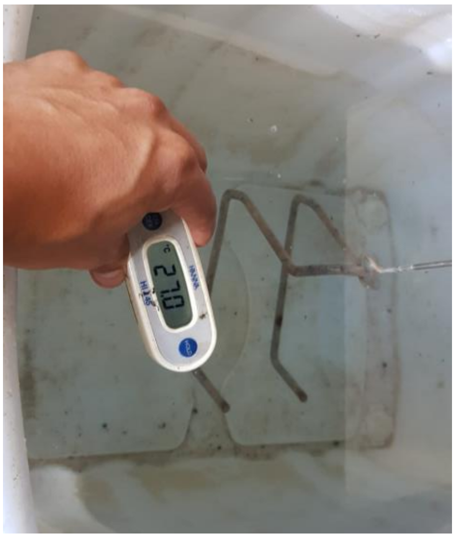

Figure 77: Measuring the test temperature

Knowing all the required mass, it was possible calculate the bulk density (SSD) of the specimen as follows:

$$\rho_{bssd} = \frac{m_1}{m_3 - m_2} \cdot \rho_w \qquad (3.10)$$

where:

m_1 is the mass of the dry specimen, in grams [g];

m_2 is the mass of the specimen in water, in grams [g];

m_3 is the mass of the saturated surface-dried specimen, in grams [g];

P_w is the density of the water, in megagrams per cubic metre [Mg/m^3].

This procedure was carried out for all the sample during the experimental campaign, in order to determinate the correction factor and evaluate the real compaction curve for each sample.

Once defined the correction factor for each sample, it was possible to determinate the result of the real compaction curve.

CHAPTER 4

Results and Discussions

4.1 Introduction

In this Chapter are reported the results of the compaction curve, VMA and VFA and the Indirect Tensile Strength obtained from the samples created during the compaction.

The goal of this Chapter is to compare the results of the different combination of mixtures obtained with the reference mixture (A/4.5/160). Since for each type of bituminous mixtures were performed several repetitions and the variation of the repetitions were limited, the comparison of the mixtures with the reference one is between the average of each type of mixtures.

4.2 Results of compaction at 160 °C

From the compaction curves in semi-logarithmic scale using a traditional method is possible to determinate two important parameters modelling the curve with a linear equation, the first parameter is the starting point of the curve that represent the auto-densification (C_1). Instead, the second parameter represent the slope of the curves, and it is called in the literature as workability (K) of the material. The value of K indicate how easy is compacted the material, in others terms with k value higher means that the asphalt mixture compacted faster.

In the following *Graph 6* is shown an example of the linear equation that model the compaction curve in semi-logarithmic scale.

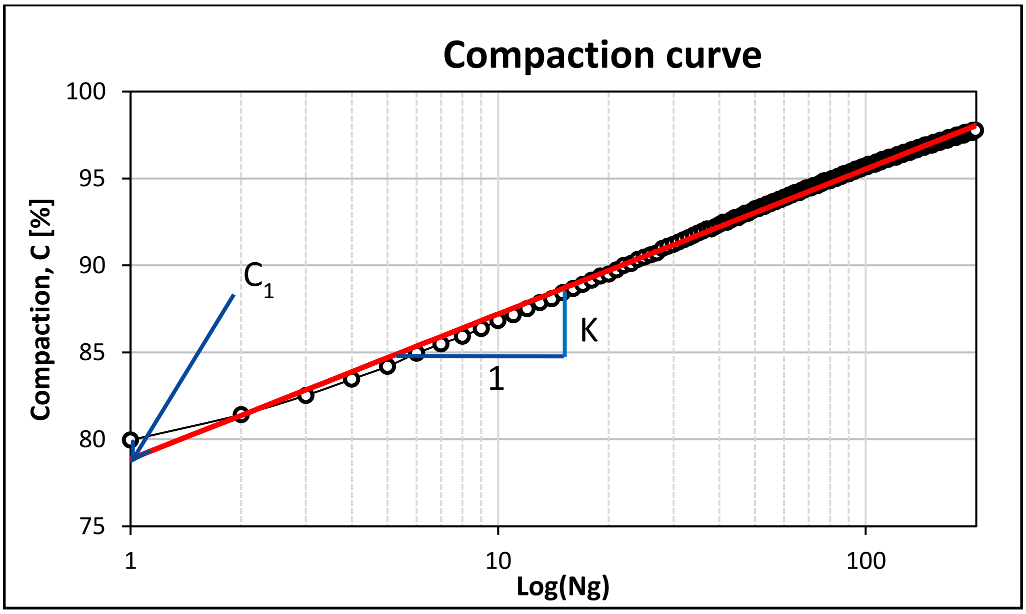

Graph 6: Example of linearization of the compaction curve

In the following section are illustrated the results of the different mixtures with the reference one.

4.2.1 Variation of the binder dosage

In this section are shown the results of the bituminous mixtures varying the binder content.

In the following *Graph 7* is illustrated the results obtained.

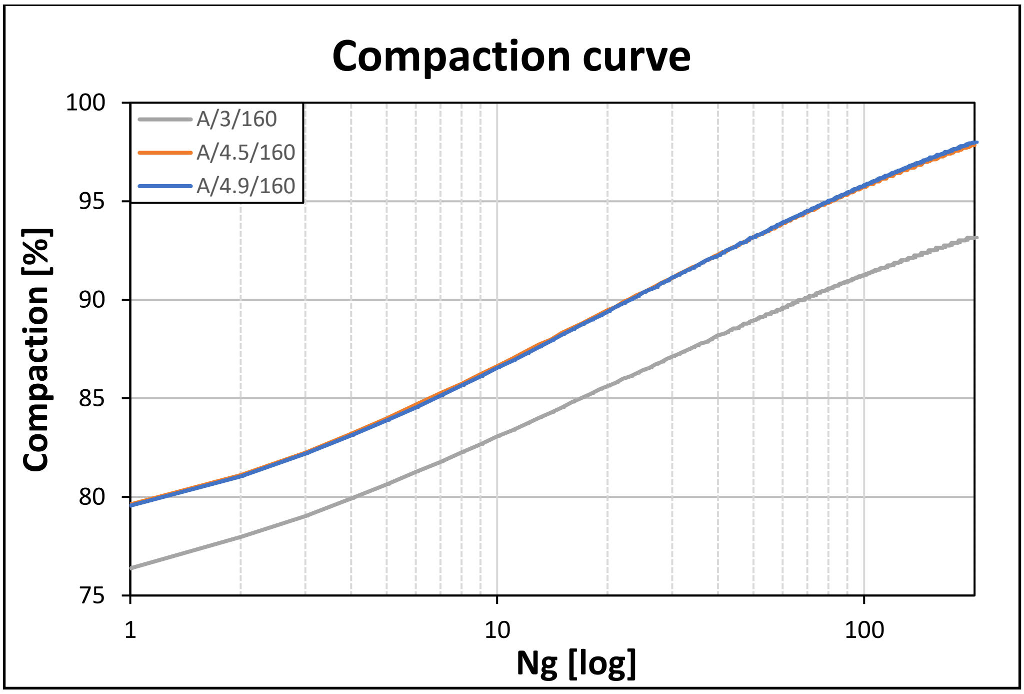

Graph 7: Compaction curves varying the binder dosage at 160 °C

From a visual interpretation, it is evident the variation of compaction passing from 4.5% of binder to 3%. Instead, a slight variation passing from 4.5% of binder to 4.9%. In this case the increment of binder is not effective the compaction behavior.

In the following *Table 12* is reported the two parameter (C_1 and K) that allows to describe the compaction curve with a linear method.

Table 12: Results of C_1 and K varying the binder content at 160 °C

Sample	C_1	K
A/3/160	75.63 %	7.76
A/4.5/160	78.48 %	8.55
A/4.9/160	78.24 %	8.71

The results of the *Table 12* shown that k increase as increase the binder content, but it is not the same trend for C_1.

4.2.2 Using the additives

In this section is illustrated the compaction curve results of the bituminous mixtures using the additives.

In the following *Graph 8* is shown the results.

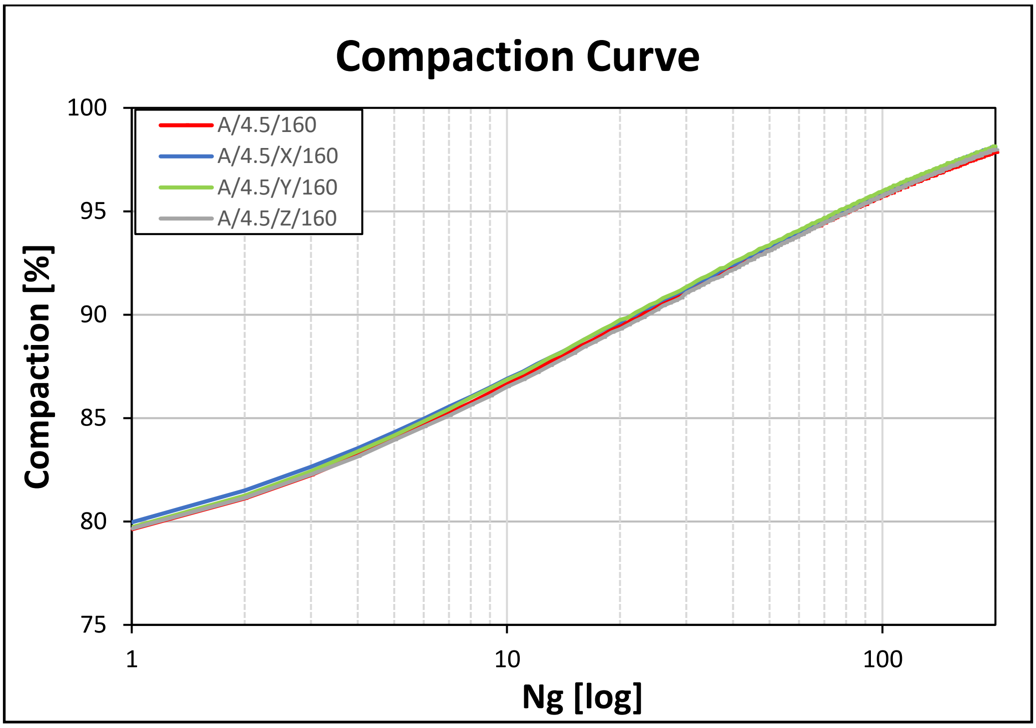

Graph 8: Compaction curve using the additives at 160°C

In this case form the Graph 8 is not evident any variation in term of compaction of the mixtures using the additives compare to the reference one. It is evident that the additives are ineffective in increase the workability of the material in this condition.

In the next *Table 13* is reported the two parameter (C_1 and K) that allows to describe the compaction curve with a linear method.

Table 13: Results of C1 and K using the additives at 160 °C

Sample	C_0	K
A/4.5/160	78.48 %	8.55
A/4.5/X/160	78.69 %	8.54
A/4.5/Y/160	78.63 %	8.61
A/4.5/Z/160	78.19 %	8.71

From the parameters C_1 and K shown similar results for all the different mixtures as shown in the *Graph 8.*

4.2.3 Changing the aggregate skeleton

In this section is reported the compaction curve changing the aggregate skeleton of the reference one.

In the following *Graph 9* is reported the result obtained.

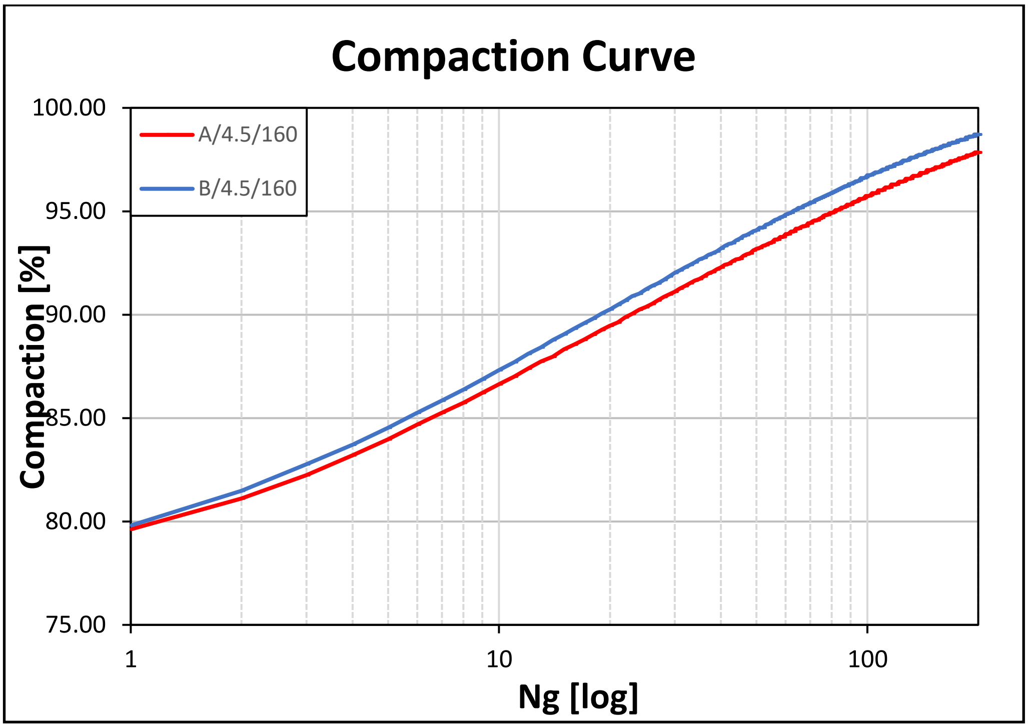

Graph 9: compaction curve changing the aggregate skeleton

From a visual consideration is evident that the composition of the aggregate skeleton B influenced the compaction phenomena due to uniforms variation of the aggregate fractions.

In the next *Table 14* is shown the result in term of C_1 and K.

Table 14: results of C_1 and K changing the aggregate skeleton at 160 °C

Sample	C_1	K
A/4.5/160	78.48 %	8.55
B/4.5/160	79.02 %	8.74

In this case both parameters (C_1 and K) are greater than the values of the reference one. It can be translated that for this test the workability can be consider greater that the reference one.

4.2.4 Summary of the results

In thus section are summarized in the following *Table 15* all the results mentioned in the previous sections.

Table 15: Summarized of the results of C1 and K at 160 °C

Sample	C_1	K
A/3/160	75.63 %	7.76
A/4.5/160	78.48 %	8.55
B/4.5/160	79.02 %	8.74
A/4.5/X/160	78.69 %	8.54
A/4.5/Y/160	78.63 %	8.61
A/4.5/Z/160	78.19 %	8.71
A/4.9/160	78.24 %	8.71

In the Table is shown that almost all the parameters (C1 and K) with 4.5% and 4.9% of binder content are similar, except the one with different aggregate skeleton (B) that shown the higher values in term of self- compaction and workability.

Instead, in the following tables are summarized the compaction curves, shown in *Table 16*, the voids content, shown in *Table 17* and the density, shown in *Table 18,* of the specimen after 10, 120, 200 gyrations of the GSC, the different rounds refer to different state of the materials:

- 10 gyrations: represent the compaction of the material subjected only to its own weight, without any type of mechanical compaction;
- 120 gyrations: represent the level of compaction of the material subjected by mechanical machines, before the opening to the traffic;
- 200 gyrations: represent the compaction of the material due to the traffic load, end life of the pavement;
-

Table 16: Results of the Compaction % C at different rounds

Sample	10 rounds	120 rounds	200 rounds
A/3/160	83.08	91.81	93.15
A/4.5/160	86.64	96.29	97.85
B/4.5/160	87.32	97.31	98.71
A/4.5/X/160	86.89	96.53	98.09
A/4.5/Y/160	86.85	96.57	98.14
A/4.5/Z/160	86.52	96.41	97.97
A/4.9/160	86.55	96.44	97.98

Table 17: Results of the voids %v at different rounds

Sample	10 rounds	120 rounds	200 rounds
A/3/160	16.92	8.19	6.85
A/4.5/160	13.36	3.71	2.15
B/4.5/160	12.68	2.69	1.29
A/4.5/X/160	13.11	3.47	1.91
A/4.5/Y/160	13.15	3.43	1.86
A/4.5/Z/160	13.48	3.59	2.03
A/4.9/160	13.45	3.55	2.02

Table 18: Results of the density at different rounds, expressed in [g/cm^3]

Sample	10 rounds	120 rounds	200 rounds
A/3/160	2.127	2.350	2.38
A/4.5/160	2.211	2.457	2.497
B/4.5/160	2.233	2.488	2.524
A/4.5/X/160	2.218	2.463	2.503
A/4.5/Y/160	2.216	2.464	2.505
A/4.5/Z/160	2.208	2.460	2.500
A/4.9/160	2.198	2.449	2.488

As it shown most of the materials have similar compaction and similar air voids except the one with low binder and the one with different aggregate skeleton. In particular, the bituminous mixture with the aggregate skeleton B present evident difference compare to the others mixtures at 120 and 200 rounds. Instead, at 10 round all the combination have similar behaviour. Regarding the one with low binder, it was expected the worst compaction due to the high reduction of binder.

In addition, in order to see better the different of compaction of the mixtures compare to the reference one, it was added one parameter computing the differences between the percentage of voids at 120 rounds of the reference mixture (A/4.5/160) and the rounds needed to have the same percentage of voids for the others mixtures. The result of the void of the reference mixture is considered equal to 3.71%.

In this way, it was possible to understand reducing effort in term of compaction for all the mixtures compare to the reference one, shown in the *Table 19*.

Table 19: Reduction of the compaction effort in term of voids

Sample	Rounds	Δ%
A/4.5/160	120	-
B/4.5/160	89	-25.83
A/4.5/X/160	111	-7.5
A/4.5/Y/160	110	-8.33
A/4.5/Z/160	116	-3.33
A/4.9/160	114	-5.0

From the *Table 19,* as expected, it is evident a considerable reduction of the effort for the mixture B/4.5/160. This mean that in this experimental campaign the variation of the aggregate skeleton influence more the compaction phenomena than the use of the additives and the increasing of the binder content.

4.3 Results of compaction at different temperatures

In this paragraph is illustrated the compaction results of the refence one (A/4.5/160) changing the temperature. To do this the test were performed two more different compaction temperature 140 and 110 °C. This type of test was performed to check how chance the compaction effect changing the temperature.

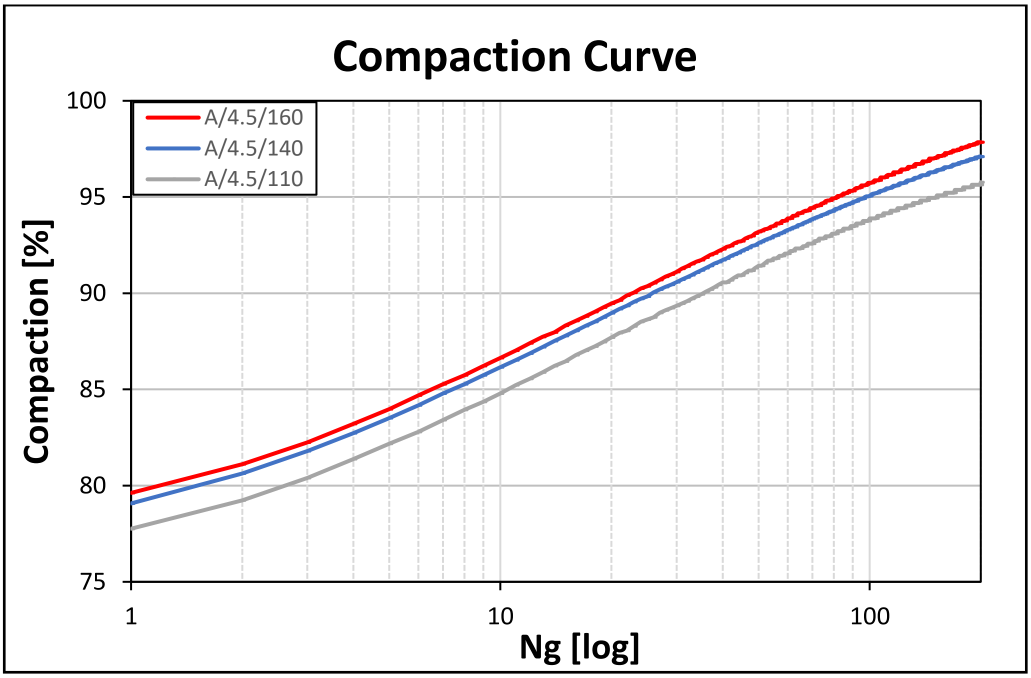

Graph 10: Compaction curves at different temperatures

In the *Graph 10* is shown, as expected, the reduction of the compaction behavior reducing the compaction temperature.

4.4 Results of VMA and VFA

The result of the voids in the mineral aggregate (VMA) are reported in the *Table 20*, in according to the standard BS EN 12697-8, mentioned in the paragraph 2.2.1.

Table 20: results of the VMA

Sample	VMA
A/4.5/160	13.60 %
B/4.5/160	12.67 %
A/4.5/X/160	13.39 %
A/4.5/Y/160	13.34 %
A/4.5/Z/160	13.51 %
A/4.9/160	14.41 %

The higher VMA is referred to the mixture A/4.9/160, it was due to the high air voids of matrix asphalt mixture and higher binder content. Instead, the lower VMA is referred to the mixture B/4.5/160, it was due to the low air voids of the matrix asphalt mixture and lower binder content.

Regarding the result of the voids in the mineral aggregate (VFA), the values are reported in the *Table 21*, in according to the standard BS EN 12697-8, mentioned in the paragraph 2.2.1.

Table 21:Results of the VFA

Sample	VFA
A/4.5/160	84.23 %
B/4.5/160	91.37 %
A/4.5/X/160	85.77 %
A/4.5/Y/160	86.07 %
A/4.5/Z/160	84.82%
A/4.9/160	85.91 %

The VFA was used to evaluate the effective asphalt thickness between aggregates. As it known too thin binder thickness was not conducive to the bonding between the mixtures. It is influenced by environmental factors, the aging of asphalt will make the performance of the mixture declined sooner, so that the service life of asphalt pavement was reduced. Instead, too thick binder thickness was not conducive to contact between aggregates, which is easy to cause insufficient strength and deformation of the mixture.

4.5 Indirect Tensile Strength (ITS)

The Indirect Tensile Strength is the test that provides a braking parameter of the material. The ITS test was performed according to BS EN 12697-23: 2017 [22].

To evaluate this test, the cylinder specimen must be placed into the compression testing machine, shown in *Figure 78*, the sample is place between the loading strips and it is loaded diametrically along the direction of the cylinder axis with a constant speed (50±2 mm/min) of displacement until it breaks.

Figure 78: ITS Static Press Machine

The ITS is the maximum indirect tensile strength calculated from the peak load applied at the breaking point of the sample. It is calculated in according to the following formula [22]:

$$ITS = \frac{2\mathrm{P}}{\pi DH} \cdot 1000 \tag{3.11}$$

where:

P is the peak load, expressed in Newton (N);

D is the diameter of the specimen, expressed in millimetres (mm);

H is the height of the specimen, expressed in millimetres (mm).

The test procedure is carried out as follows:

- The first step was to put the specimen inside the climate chamber at 25 °C for at least 2 hours, this phase is called conditioning of the sample, *Figure 79;*

Figure 79: Climate chamber

- Then it was taken out the conditioned sample and placed it aligned on the load strip, as shown in *Figure 80*;

Figure 80: Sample placed for the test

- once the specimen was placed, started the test of the sample with a constant speed load until the specimen broken, as shown in *Figure 81*;

Figure 81: Sample broken

- at the end it was recorded also the type of failure according to the *Figure 82*.

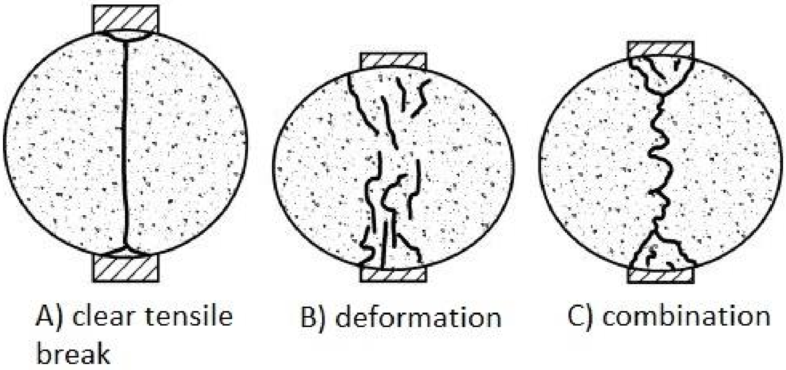

Figure 82: Type of failure

The results of the test are summarized in the following *Table 22*.

Table 22: Results of the ITS test

Design grain size	**ITS [MPa]**	**Type of failure**
A/4.5/160	1.474	A
B/4.5/160	1.661	A
A/4.5/X/160	1.202	A
A/4.5/Y/160	1.176	A
A/4.5/Z/160	1.237	A
A/4.9/160	1.367	A

The results shown that the ITS value for the mixtures with the additives it is affected by the additive itself. The main reason for the reduction of the ITS value is caused by the oil present in the additive that it reduced the grip between the aggregates.

Furthermore, in the *Graph 11* is shown the ITS result in function of the vertical deformation.

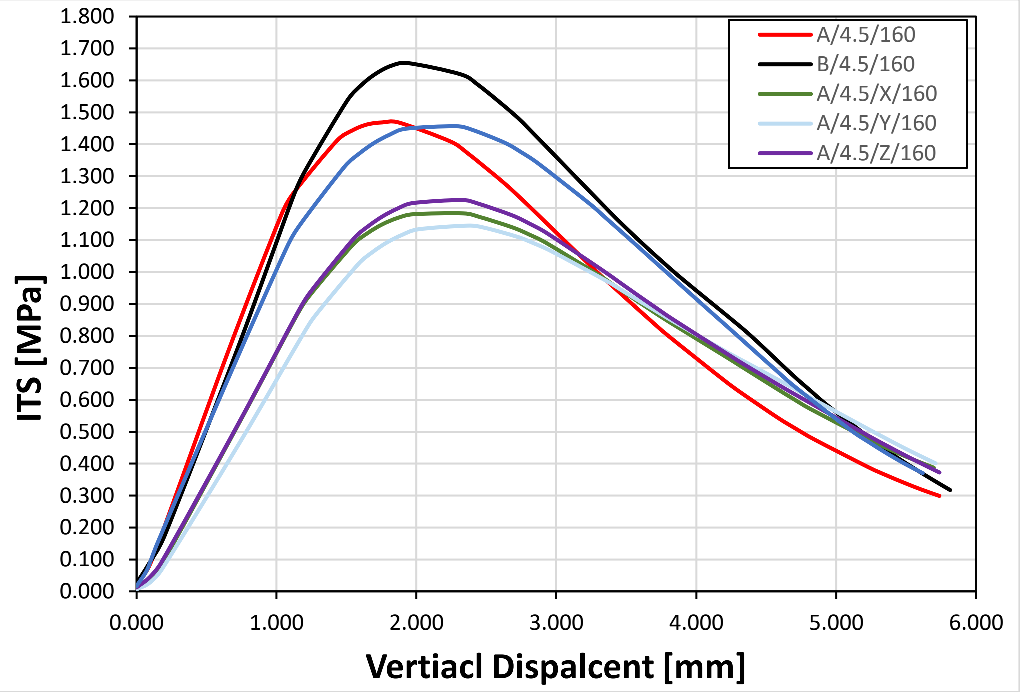

Graph 11: ITS diagram in function of the displacement

From the *Graph 11*, it is evident that the samples with the additives present longer vertical deformation before failure, due to the effect of the additive that made soft the binder compare to the refence one. Instead, the mixture with the different aggregate skeleton lower vertical deformation, but higher ITS value.

In order to complete the information about the mechanical properties of each material, it been evaluated also the Indirect Tensile Coefficient (CTI) using the follow equation:

$$CTI = \frac{\pi}{2} \cdot \frac{\mathrm{D} \cdot ITS}{D_c} \tag{3.12}$$

where:

ITS is the Indirect Tensile Strength, expressed in megapascals (MPa);

D is the diameter of the specimen, expressed in millimetres (mm);

D_c is the vertical displacement, expressed in millimetres (mm).

The results are illustrated in the following *Table 23*.

Table 23: Results of the CTI

Design grain size	**ITC [MPa]**
A/4.5/160	140.645
B/4.5/160	146.247
A/4.5/X/160	97.096
A/4.5/Y/160	90.204
A/4.5/Z/160	96.233
A/4.9/160	110.446

CHAPTER 5

Analytical Models

5.1 Introduction

The objective of this chapter is to find a model that can simulate the whole compaction curve of the compaction test performed. To do this, different analytical models were analysed to find the better solution.

A mechanical model is a mathematical simplification of quite complex physical behaviour, the main aim is to define a model that is sufficiently accurate, but not too complex, otherwise, the physical meaning of the material is lost.

In this study each mechanical model is represented by a constitutive equation expressed in a closed-form. The objective of the model equation is to try to fit the compaction curves of the compaction test performed, minimizing the difference with the real compaction curve obtained from the GSC in the Chapter 4 and the model compaction curve.

The solution of the constitutive equation of the model is obtained from a constant load, thus the load that simulate the action given by the GSC is a constant load. In the reality a constant load cannot simulate the action given by the GSC, but for this study in order to make easy the solutions of the models and their computation a constant load was chosen.

After defined the analytic equation of the model and the load, the models were implemented in Excel, that is a software program created by Microsoft that uses spreadsheets to organize numbers, data formulas and functions. Through the SOLVER implemented in excel was possible minimize the difference between the real compaction curve and the model compaction curve. It modifies one or more cells containing numeric values (variable cells) to find a solution to a cell (Objective cell) containing a formula that recalls, within it, the data off the variable cells [23].

5.2 Analytical models

Knowing the theory of simple models from the paragraph 2.5, now it is possible to create complex arrangements combining different simple model, then solve the mathematical equations, implement in excel and compare the results with the real measures.

In this section will be analysed different models that were implemented to determinate the better solution, reducing the difference with the model compaction curves and the one obtained with the GSC.

5.2.1 Spring plus Kelvin-Voight in series

The first tentative is a model composed by a spring, with elastic modulus equal to E_0, linked with Kelvin-Voight model, connected in series, as shown in *Figure 83.*

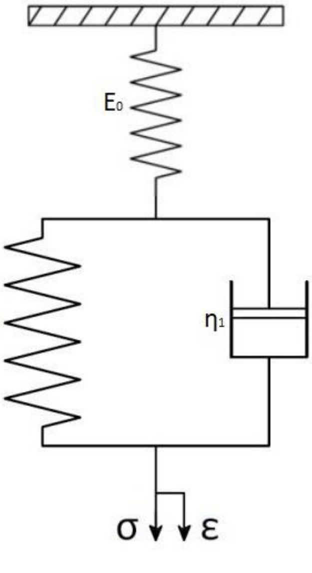

Figure 83: Spring plus kelvin-Voight model in series

This model is characterized by the following fundamental laws:

$$\sigma = \sigma_S = \sigma_K \tag{4.1}$$

$$\varepsilon = \varepsilon_S + \varepsilon_K \tag{4.2}$$

(4.1) and (4.2) are the basic equation that control the model, deriving and combining them it is possible to obtain the constitutive law of the system.

$$\dot{\varepsilon} = \dot{\varepsilon_S} + \dot{\varepsilon_K} \tag{4.3}$$

Where:

$$\dot{\varepsilon_S} = \frac{\dot{\sigma}}{E_0} \tag{4.4}$$

$$\dot{\varepsilon_K} = \frac{\sigma}{\eta_1} - \frac{E_1 \cdot \varepsilon_K}{\eta_1} \tag{4.5}$$

Substituting equation (4.4) and (4.5) into (4.3):

$$\dot{\varepsilon} = \frac{\dot{\sigma}}{E_0} + \frac{\sigma}{\eta_1} - \frac{E_1 \cdot \varepsilon_K}{\eta_1} \tag{4.6}$$

Rearranging (4.6), the generalized equation is:

$$\dot{\varepsilon} + \frac{E_1 \cdot \varepsilon_K}{\eta_1} = \frac{\dot{\sigma}}{E_0} + \frac{\sigma}{\eta_1} \tag{4.7}$$

The solution of (4.7) has the following form for creep under a constant stress σ_0:

$$\varepsilon = \frac{\sigma_0}{E_0} + \frac{\sigma_0}{E_1} \cdot (1 - e^{-E_1 \cdot t / \eta_1}) \tag{4.8}$$

Thus, the initial strain at t=0 is given by the spring element, $\varepsilon(0) = \frac{\sigma_0}{E_0}$, then increases with a decreasing rate and approaches asymptotically the value of $\frac{\sigma_0}{E_0} + \frac{\sigma_0}{E_1}$ when t tends to infinity. The response after t > 0 of this model to an abruptly applied stress is that the stress is at first carried entirely by the viscous element (η_1) in the Kelvin-Voight model. The viscous element tends to elongates under the stress, thus transferring a greater and greater portion of the load to the elastic element E_1. Under t infinity the entire stress is carried by the elastic element. This behavior just described is appropriately called delayed elasticity [24].

The strain rate $\dot{\varepsilon}$ for this model in creep under constant stress σ_0 is found by differentiating (4.8):

$$\dot{\varepsilon} = \frac{\sigma_0}{\eta_1} \cdot e^{-E_1 \cdot t / \eta_1} \tag{4.9}$$

The initial strain rate at $t=0^+$ is finite, $\dot{\varepsilon}\ (0^+) = \frac{\sigma_0}{\eta_1}$, and the strain rate approaches asymptotically to the value $\dot{\varepsilon}\ (\infty) = 0$ when t tends to infinity.

Considering the Kelvin-Voight element, if the stress were to increase at its initial rate $\frac{\sigma_0}{\eta_1}$, it would cross the asymptotic line at time $t_c = \frac{\eta_1}{E_1}$, called the retarding time. Actually, most of the strain ε_K occurs within the retardation time period since

$e^{-E_1 \cdot t / \eta_1}$ converges toward the asymptotic value rapidly for t<t$_c$. At t=t$_c$, $\varepsilon_K = \frac{\sigma_0}{E_1} \cdot \left(1 - \frac{1}{e}\right) = 0.63 \cdot \frac{\sigma_0}{E_1}$. Thus, only the 37% of the asymptotic strain ε_K remains to be accomplished after t=t$_c$ [24].

The creep and recovery response are shown in the following *Figure 84* and *85.*

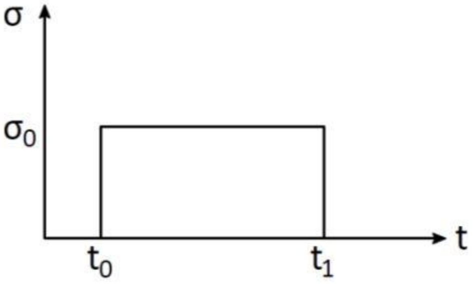

Figure 84: Creep and Recovery test/ Spring+Kelvin in series - Stress

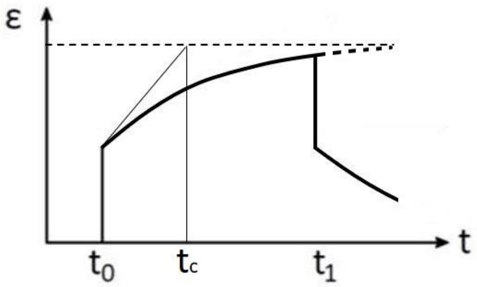

Figure 85: Creep and Recovery test/ Spring+Kelvin in serie - Strain

5.2.2 Generalized Kelvin-Voight

The generalized Kelvin-Voight model connected in series, shown in *Figure 86*, is convenient for viscoelastic analysis, due to the fact that the stress history is prescribed. This model should permit a close description of real behavior of the material.

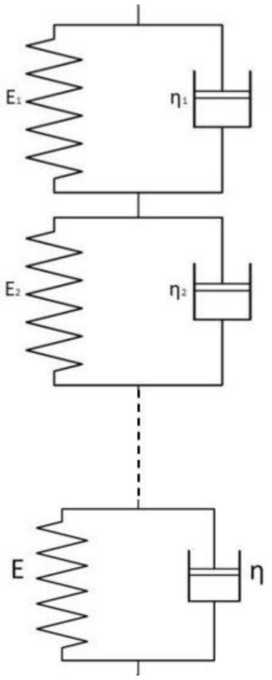

Figure 86: Generalized Kelvin-Voight model in series

Spring plus two Kelvin-Voight model in series

This model is composed by a spring, with elastic modulus equal to E_0, connected at two Kelvin-Voight model in series, as shown in *Figure 87*. In this model as the one in the previous paragraph, the spring is added in order the best representation of the material, since the auto-densification is carried out by the spring.

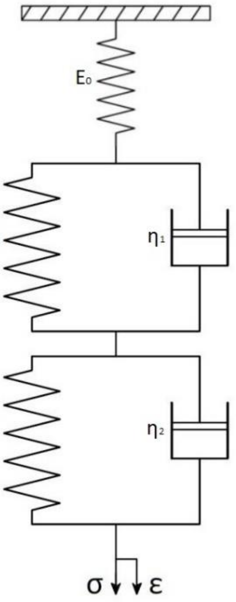

Figure 87: Spring plus two Kelvin-Voight in series

The fundamental laws of this model are:

$$\sigma = \sigma_S = \sigma_{K_1} = \sigma_{K_2} \tag{4.10}$$

$$\varepsilon = \varepsilon_S + \varepsilon_{K_1} + \varepsilon_{K_2} \tag{4.11}$$

These are the condition equations that control the model, deriving and combining them it is possible to obtain the constitutive law of the system.

$$\dot{\varepsilon} = \dot{\varepsilon_S} + \dot{\varepsilon_{K_1}} + \dot{\varepsilon_{K_2}} \tag{4.12}$$

Where:

$$\dot{\varepsilon_M} = \frac{\dot{\sigma}}{E_0} \tag{4.13}$$

$$\dot{\varepsilon_{K_1}} = \frac{\sigma}{\eta_1} - \frac{E_1 \cdot \varepsilon_{K_1}}{\eta_1} \tag{4.14}$$

$$\dot{\varepsilon_{K_2}} = \frac{\sigma}{\eta_2} - \frac{E_2 \cdot \varepsilon_{K_2}}{\eta_2} \tag{4.15}$$

Substituting equation (4.13), (4.14) and (4.15) into (4.12):

$$\dot{\varepsilon} = \frac{\dot{\sigma}}{E_0} + \frac{\sigma}{\eta_1} - \frac{E_1 \cdot \varepsilon_{K_1}}{\eta_1} + \frac{\sigma}{\eta_2} - \frac{E_2 \cdot \varepsilon_{K_2}}{\eta_2} \tag{4.16}$$

Rearranging the equation (4.16), the generalized equation is:

$$\dot{\varepsilon} + \frac{E_1 \cdot \varepsilon_{K_1}}{\eta_1} + \frac{E_2 \cdot \varepsilon_{K_2}}{\eta_2} = \frac{\dot{\sigma}}{E_0} + \frac{\sigma}{\eta_1} + \frac{\sigma}{\eta_2} \tag{4.17}$$

The solution of (4.17) under constant stress σ_0 can be obtained directly, by considering that the total strain is the sum of the creep strain of each individual Kelvin-Voight model. Thus, the creep strain of this model has the following form [24]:

$$\varepsilon = \frac{\sigma_0}{E_0} + \sigma_0 \sum_{i=1}^{2} \phi_i \cdot \left(1 - e^{-t/t_e^i}\right) \tag{4.18}$$

where:

$\phi_i=1/E_i$ *is the reciprocal modulus;*

$t_c^i = \eta_i/E_i$ *is the retardation time;*

Spring plus three Kelvin-Voight model in series

The structure of this model and the concept are the same of the previous one, the only difference is an additional Kelvin-Voight model, as shown in *Figure 88*.

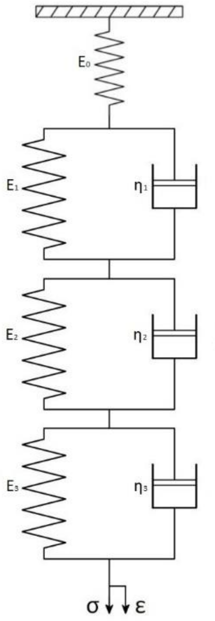

Figure 88: Spring plus three Kelvin-Voight model in series

The fundamental laws of this model are:

$$\sigma = \sigma_S = \sigma_{K_1} = \sigma_{K_2} = \sigma_{K_3} \tag{4.19}$$

$$\varepsilon = \varepsilon_S + \varepsilon_{K_1} + \varepsilon_{K_2} + \varepsilon_{K_3} \tag{4.20}$$

These are the condition equations that control the model, deriving and combining them it is possible to obtain the constitutive law of the system.

$$\dot{\varepsilon} = \dot{\varepsilon_S} + \dot{\varepsilon_{K_1}} + \dot{\varepsilon_{K_2}} + \dot{\varepsilon_{K_3}} \tag{4.21}$$

Where:

$$\dot{\varepsilon_M} = \frac{\dot{\sigma}}{E_0} \tag{4.22}$$

$$\dot{\varepsilon_{K_1}} = \frac{\sigma}{\eta_1} - \frac{E_1 \cdot \varepsilon_{K_1}}{\eta_1} \tag{4.23}$$

$$\dot{\varepsilon_{K_2}} = \frac{\sigma}{\eta_2} - \frac{E_2 \cdot \varepsilon_{K_2}}{\eta_2} \tag{4.24}$$

$$\dot{\varepsilon_{K_3}} = \frac{\sigma}{\eta_3} - \frac{E_3 \cdot \varepsilon_{K_3}}{\eta_3} \tag{4.25}$$

Substituting equation (4.22), (4.23), (4.24) and (4.25) into (4.21):

$$\dot{\varepsilon} = \frac{\dot{\sigma}}{E_0} + \frac{\sigma}{\eta_1} - \frac{E_1 \cdot \varepsilon_{K_1}}{\eta_1} + \frac{\sigma}{\eta_2} - \frac{E_2 \cdot \varepsilon_{K_2}}{\eta_2} + \frac{\sigma}{\eta_2} - \frac{E_2 \cdot \varepsilon_{K_2}}{\eta_2} \quad (4.26)$$

Rearranging the equation (4.26), the generalized equation is:

$$\dot{\varepsilon} + \frac{E_1 \cdot \varepsilon_{K_1}}{\eta_1} + \frac{E_2 \cdot \varepsilon_{K_2}}{\eta_2} + \frac{E_3 \cdot \varepsilon_{K_3}}{\eta_3} = \frac{\dot{\sigma}}{E_0} + \frac{\sigma}{\eta_1} + \frac{\sigma}{\eta_2} + \frac{\sigma}{\eta_3} \quad (4.27)$$

The solution of (4.27) under constant stress σ_0 is the same as the previous model, thus the creep strain of this model has the following form:

$$\varepsilon = \frac{\sigma_0}{E_0} + \sigma_0 \sum_{i=1}^{3} \phi_i \cdot \left(1 - e^{-t/t_e^i}\right) \quad (4.28)$$

where:

$\phi_i = 1/E_i$ is the reciprocal modulus;

$t_c^i = \eta_i/E_i$ is the retardation time;

5.3 Assumptions of the models

In this section is mentioned some necessary assumptions that allows to use the developed models for the purpose of this study.

The main assumptions, it is to assume the spring element not like a normal spring, but consider a spring that work only in one direction. In this way the spring element after the loading cannot return back to its initial position. Even the new spring is not acting like the normal spring, its constitutive equation is respecting the Hook law. In this way the equation of the developed models remains the same and thus at the end of the compaction test, when the load is removed, the new spring element is keeping the deformation.

These assumptions assumed guarantee a real description of the behavior of the material. Otherwise, at the end of the test after remove the load the deformation of the spring is returning back immediately and also the deformation by the Kelvin-Voight element are returning back considering a long time.

5.4 Model computations

The analysis starts with the implementation of the model equation in the computing environment, then, a constant stress was implemented is equal to 600 kPa, that it is the load that simulate the action of the GSC.

Once defined the equation and the load, the objective of this part was to obtain a set of parameters that allows to build the model compaction curve, in a way to minimize the distance between the real one.

To do this, the solver in excel were used, shown in *Figure 89*, as follows:

- selected the goal, that is the cell that contains the result between the model compaction and the real one to power two, and clicked its minimization;
- then selected the variables of the models, this variable are the parameters that the solver will find minimizing the result of the goal, that mean the best fitting;
- as last step it is necessary to add some constrains, all the variable of the models need to be greater than 1.
- once everything is set follows the running process, the solver returns an optimal solution.

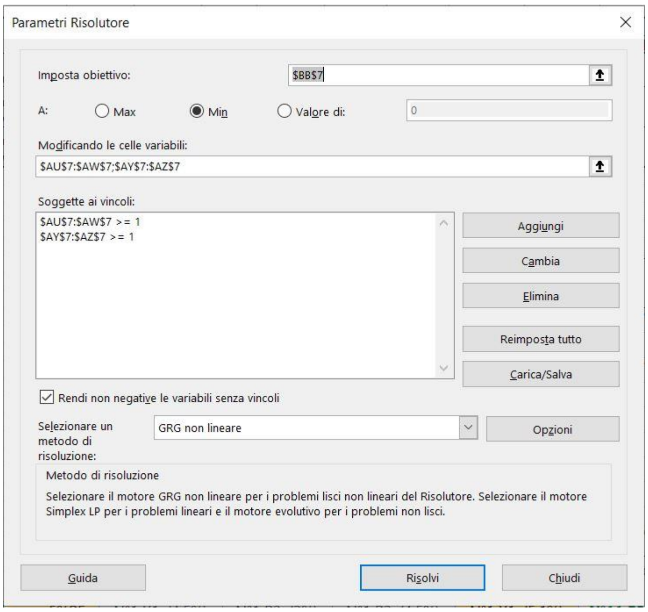

Imposta obiettivo: $BB$7

A: ○ Max ● Min ○ Valore di: 0

Modificando le celle variabili:
$AU$7:$AW$7;$AY$7:$AZ$7

Soggette ai vincoli:
$AU$7:$AW$7 >= 1
$AY$7:$AZ$7 >= 1

☑ Rendi non negative le variabili senza vincoli

Selezionare un metodo di risoluzione: GRG non lineare

Metodo di risoluzione

Selezionare il motore GRG non lineare per i problemi lisci non lineari del Risolutore. Selezionare il motore Simplex LP per i problemi lineari e il motore evolutivo per i problemi non lisci.

Figure 89: Setting the Solver

The implementation of the models started from the simulation of the compaction curve of the reference mixture (A/4.5/160), using the models analysed in the paragraph 4.2.

Once obtained the solutions of the models, the following step was to select the one that simulate with high accuracy the real compaction curve and respect the physical meaning of the material.

In the following is shown *Table 24* is shown the parameters of the models.

Table 24: Model's parameters of A/4.5/160

Model	E_0	E_1	E_2	η_1	η_2	η_3	RMS
Spring + 1 Kelvin	7.32	39.70		1422.42			89.50
Spring + 2 Kelvin	7.73	53.70	63.95	3505.42	390.02		3.88
Spring + 3 Kelvin	7.82	61.15	131.78	5181.46	247.33	980.93	0.40

From the parameters of the model is possible to graph the model compactions curves, as shown in *Graph 12*, in logarithmic scale, and *13*, in normal scale.

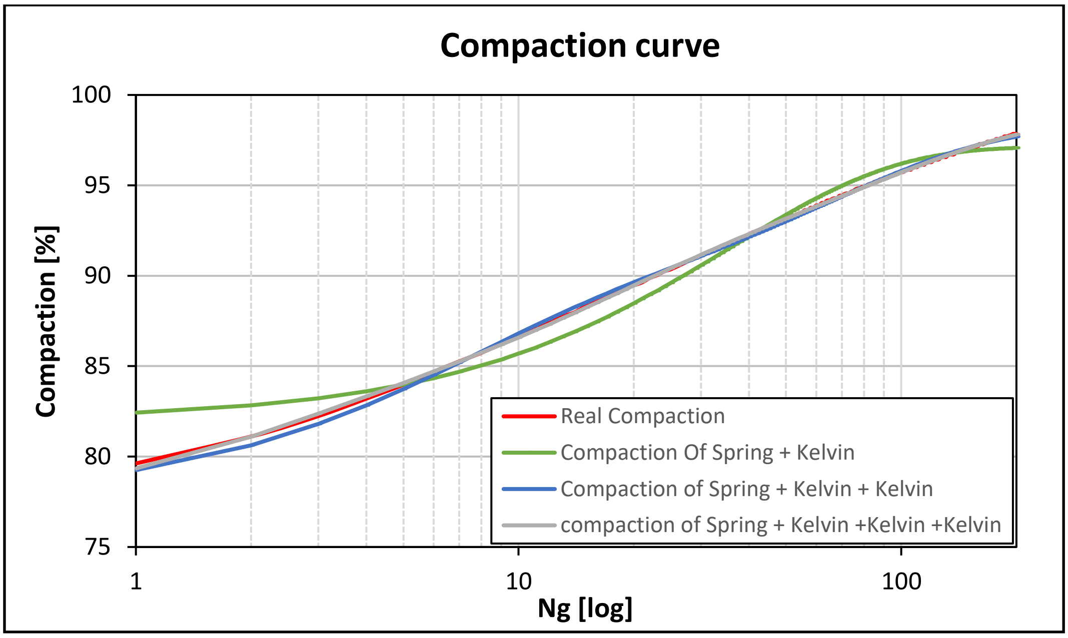

Graph 12: Results of model compaction curve of the reference mixture A/4.5/160, in semi-logarithmic scale

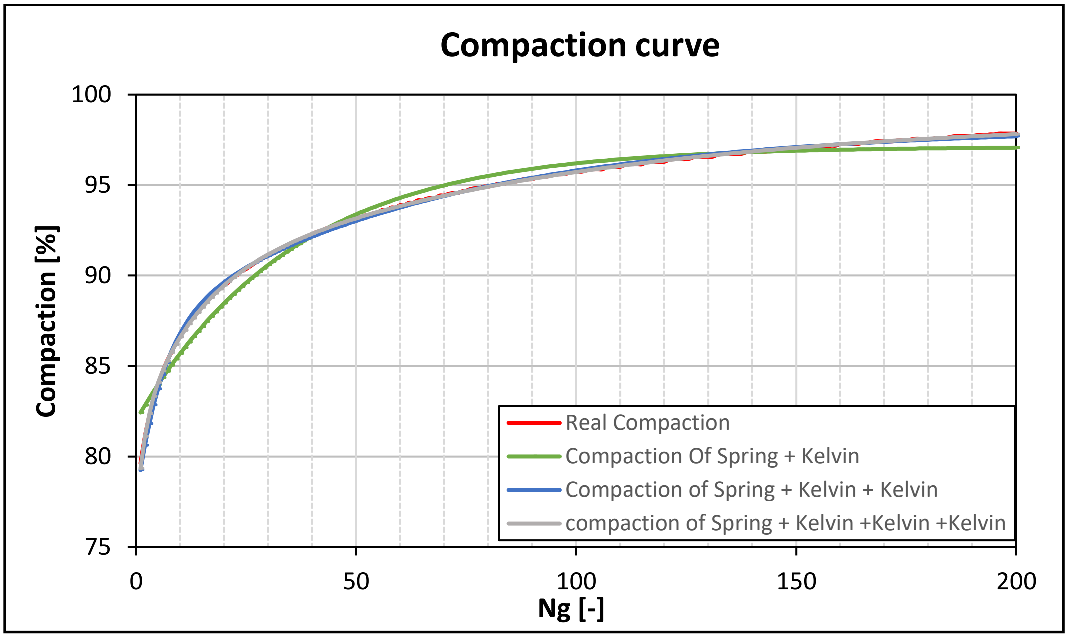

Graph 13: Results of model compaction curve of the reference mixture A/4.5/160, in normal scale

From the *Graph 12* and *13,* it is evident that the model compose by the Spring and one Kelvin element in series doesn't fit with enough accuracy the real compaction, there is a clear fluctuation around the real compaction curve. Instead, the model is composed by the Spring and three Kelvin elements is fitting with the higher accuracy the real compaction curve, but its elements increase the complexity of the model and was difficult define a physical meaning of the material.

From these considerations the choice went to the model compose by the Spring and two Kelvin-Voight elements. Even the accuracy is not high as the one with three kelvin elements, it simulates with enough accuracy the compaction curve.

Once select the representative model (Spring + 2 Kelvin), it is been possible implement all the obtained compaction curves for all the different mixtures.

In the followings section are illustrated the result of the simulated curves and comparison for all the asphalt mixture with the reference one at 160 °C of compaction and the mixtures at different compaction temperature.

5.4.1 Result of the simulation at the same compaction T

In this paragraph is illustrated the result of the model parameters, shown in the tables, and the graphs of the model compaction curves, in logarithmic and normal scale, compacted at 160 °C of compaction.

Table 25: Model's parameters of B/4.5/160

Model	E_0	E_1	E_2	η_1	η_2	RMS
Spring + 2 Kelvin	7.73	52.36	61.00	3160.40	350.11	4.41

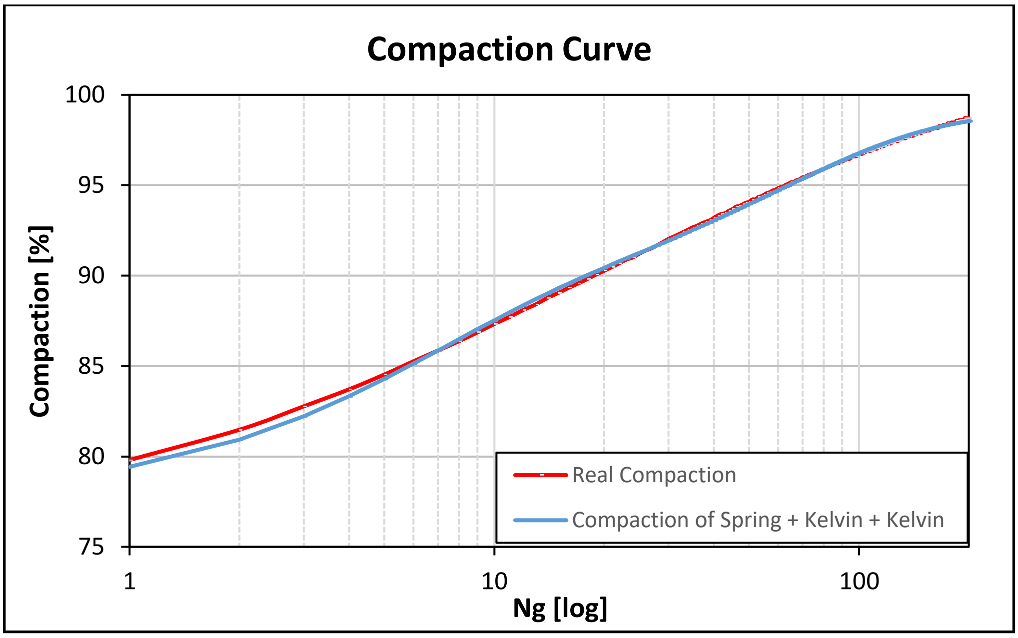

Graph 14: Model compaction curve of B/4.5/160, in semi-logarithmic scale

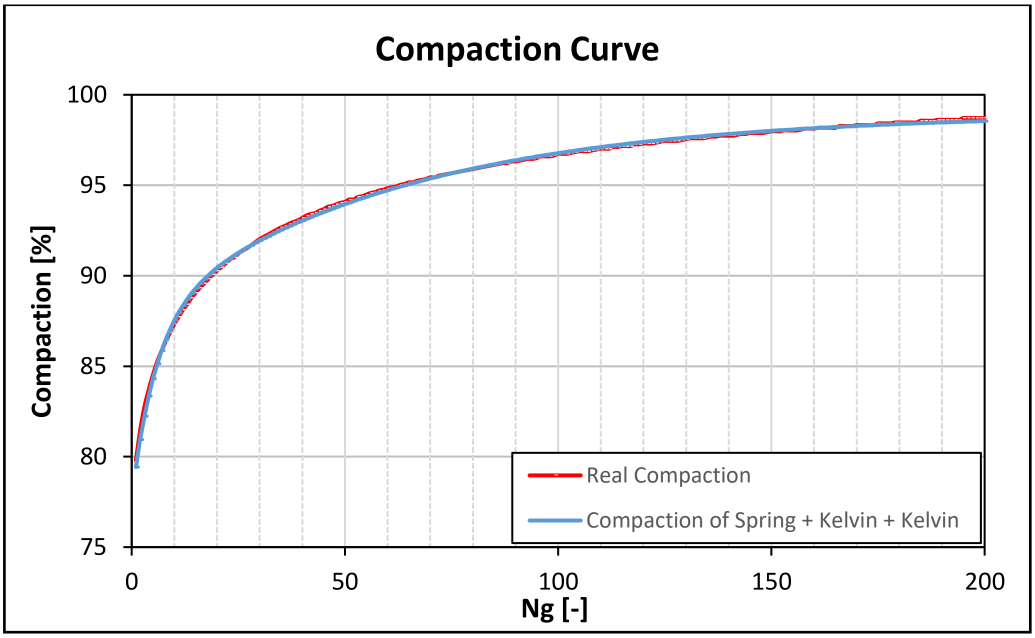

Graph 15: Model compaction curve of B/4.5/160, in normal scale

Table 26: Model's parameters of A/4.5/X/160

Model	E_0	E_1	E_2	η_1	η_2	RMS
Spring + Kelvin + Kelvin	7.69	53.00	65.58	3520.63	387.82	3.86

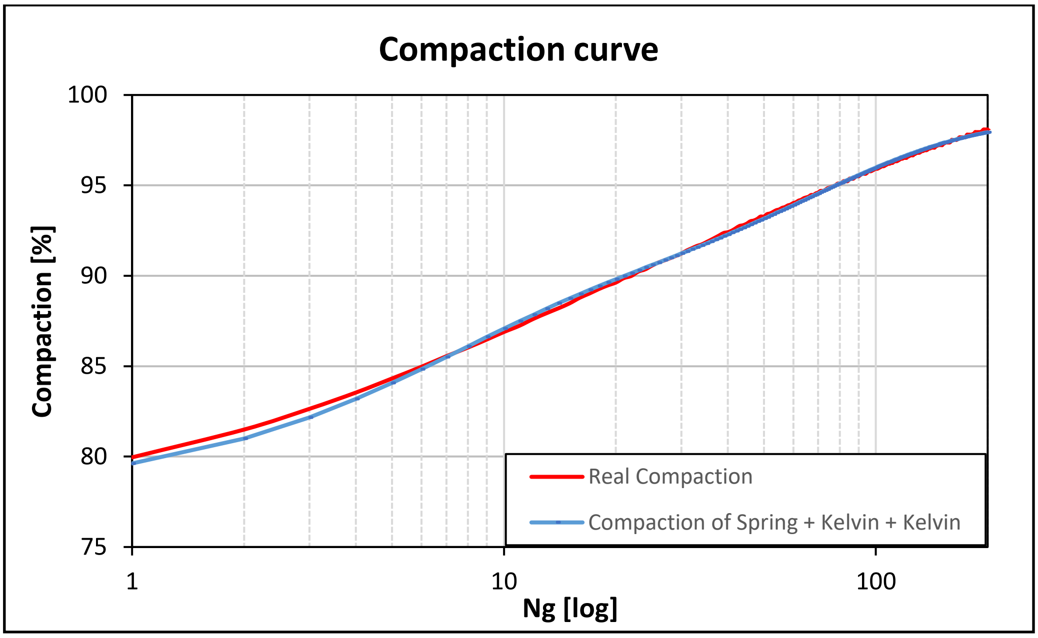

Graph 16: Model compaction curve of A/4.5/X/160, in semi-logarithmic scale

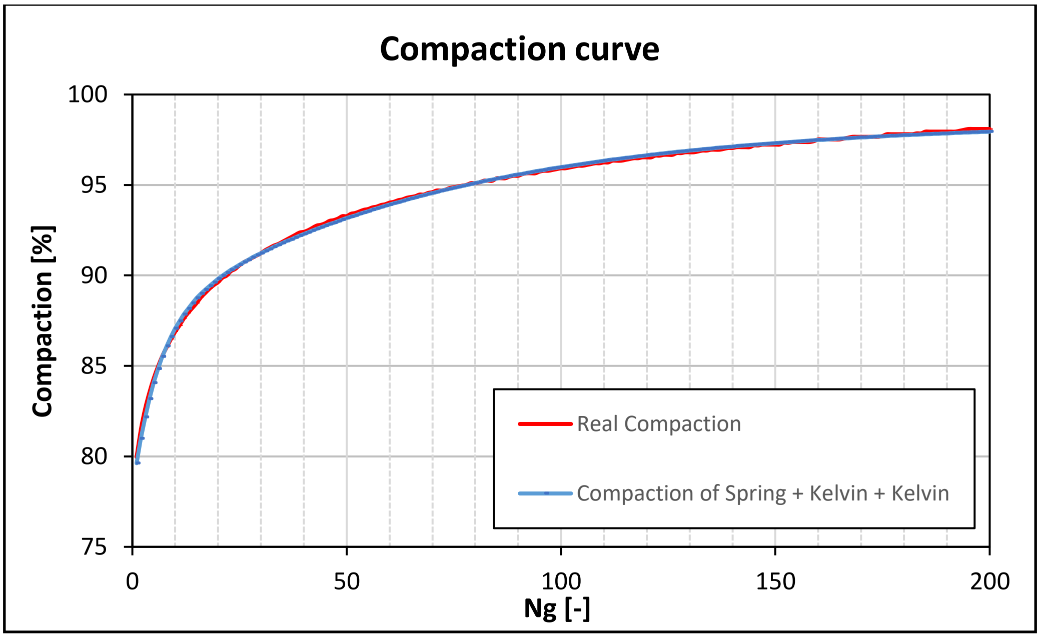

Graph 17: Model compaction curve of A/4.5/X/160, in normal scale

Table 27: Model's parameters of A/4.5/Y/160

Model	**E_0**	**E_1**	**E_2**	**η_1**	**η_2**	**RMS**
Spring + 2 Kelvin	7.71	53.58	62.91	3552.42	386.96	3.80

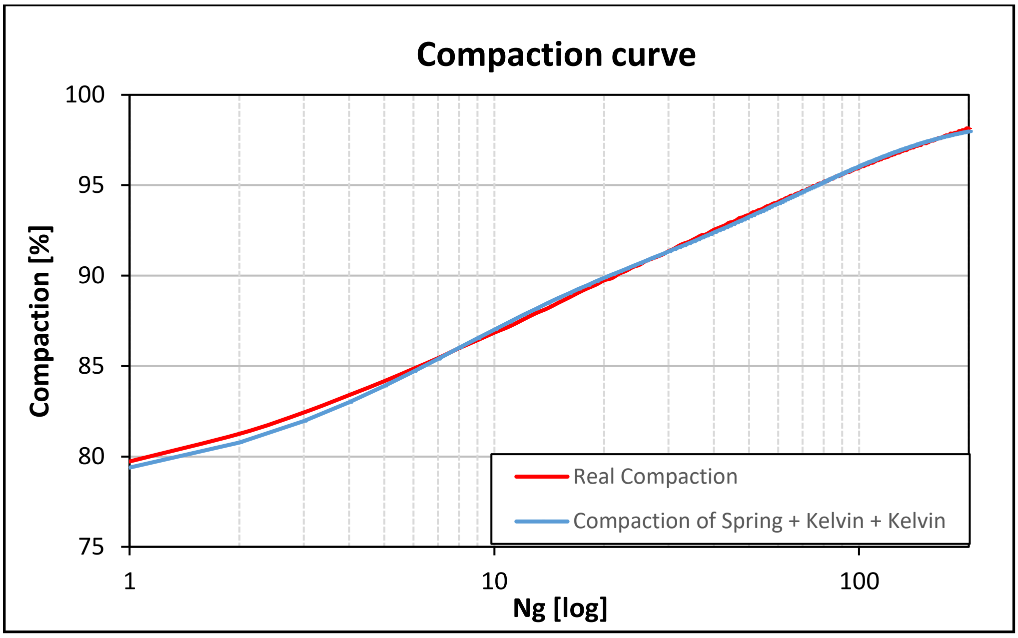

Graph 18: Model compaction curve of A/4.5/Y/160, in semi-logarithmic scale

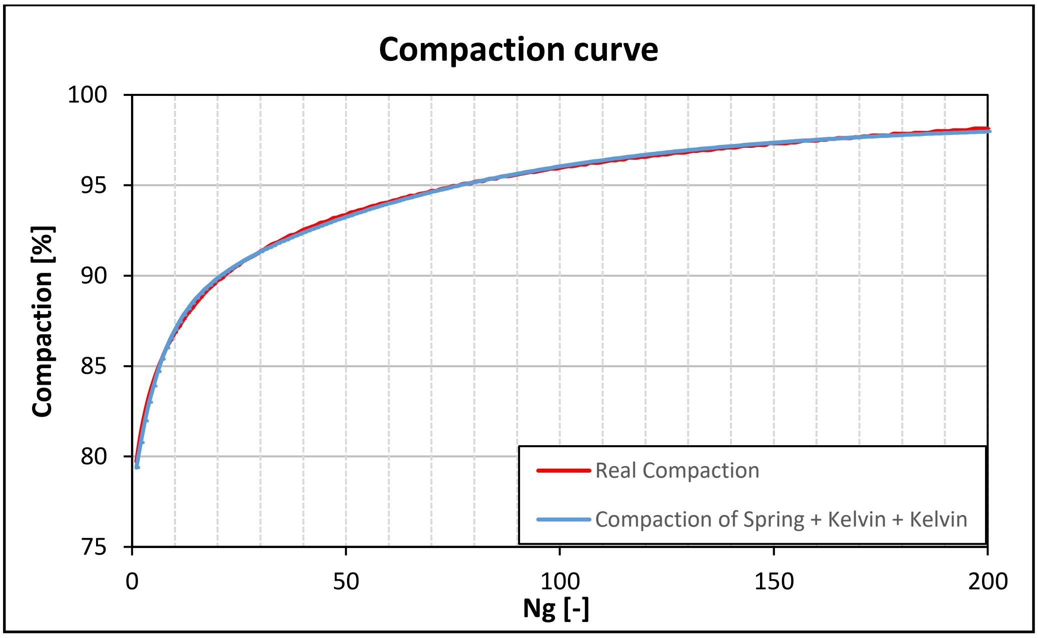

Graph 19: Model compaction curve of A/4.5/Y/160, in normal scale

Table 28: Model's parameters of A/4.5/Z/160

Model	E_0	E_1	E_2	η_1	η_2	RMS
Spring + 2 Kelvin	7.71	52.11	66.35	3447.64	412.85	4.12

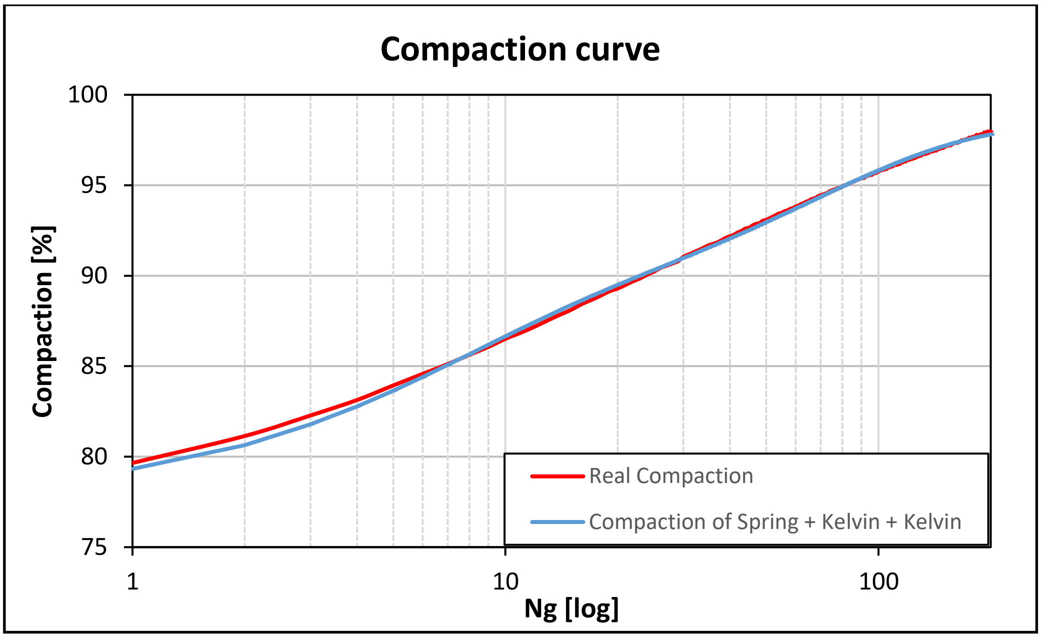

Graph 20: Model compaction curve of A/4.5/Z/160, in semi-logarithmic scale

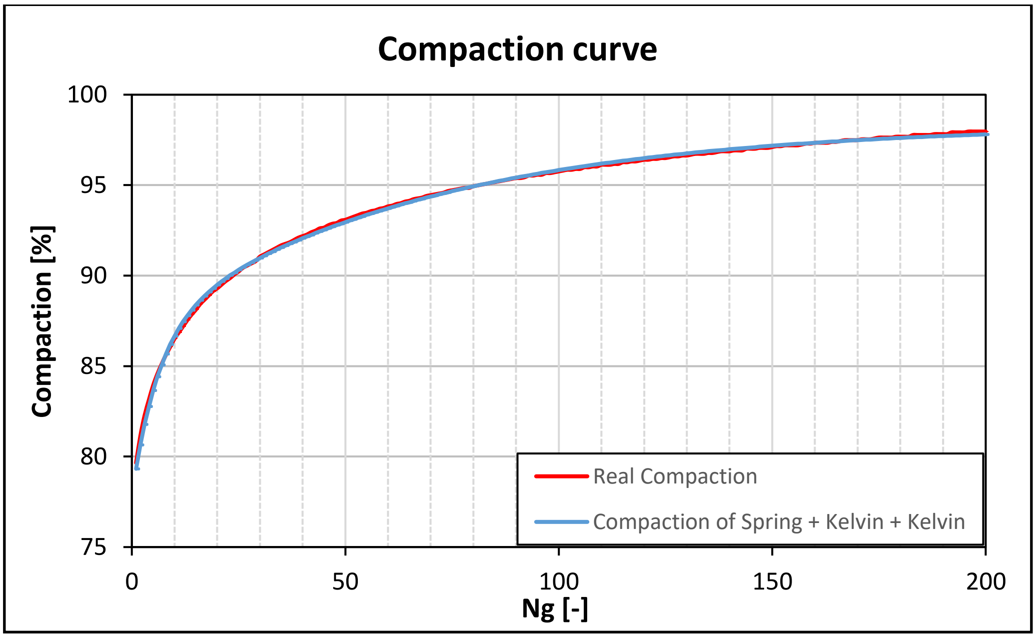

Graph 21: Compaction curve modelled of A/4.5/Z/160, in normal scale

Table 29: Model's parameters of A/4.9/160

Model	E_0	E_1	E_2	η_1	η_2	RMS
Spring + 2 Kelvin	7.72	52.83	63.51	3452.16	397.53	4.11

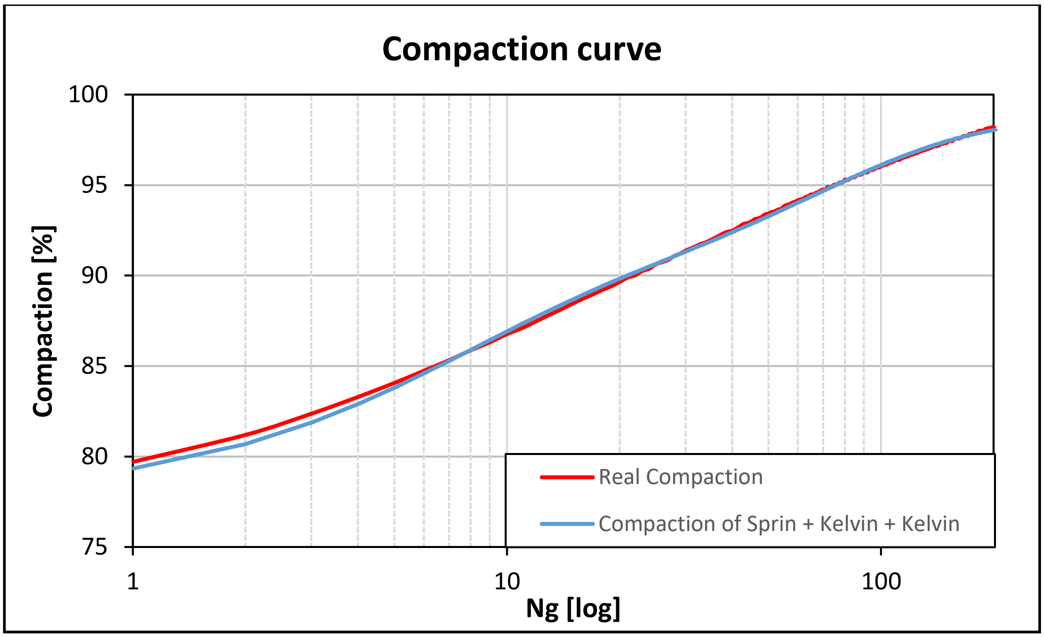

Graph 22: Compaction curve modelled of A/4.9/160, in semi-logarithmic scale

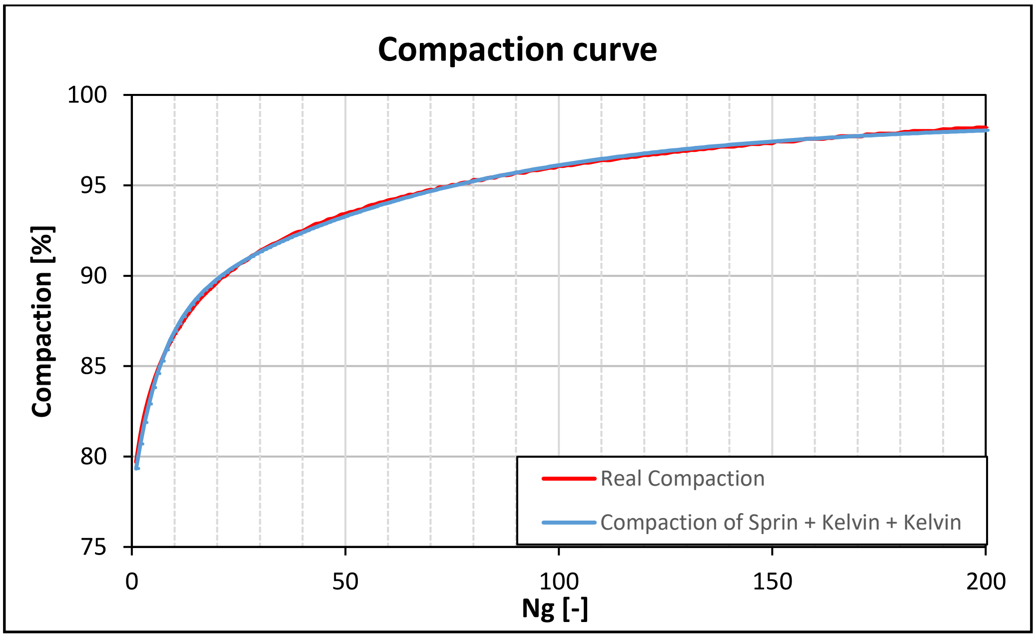

Graph 23: Compaction curve modelled of A/4.9/160, in normal scale

Table 30: Model's parameters of A/3/160

Model	E_0	E_1	E_2	η_1	η_2	RMS
Spring + 2 Kelvin	8.06	58.69	67.80	3729.33	377.04	4.16

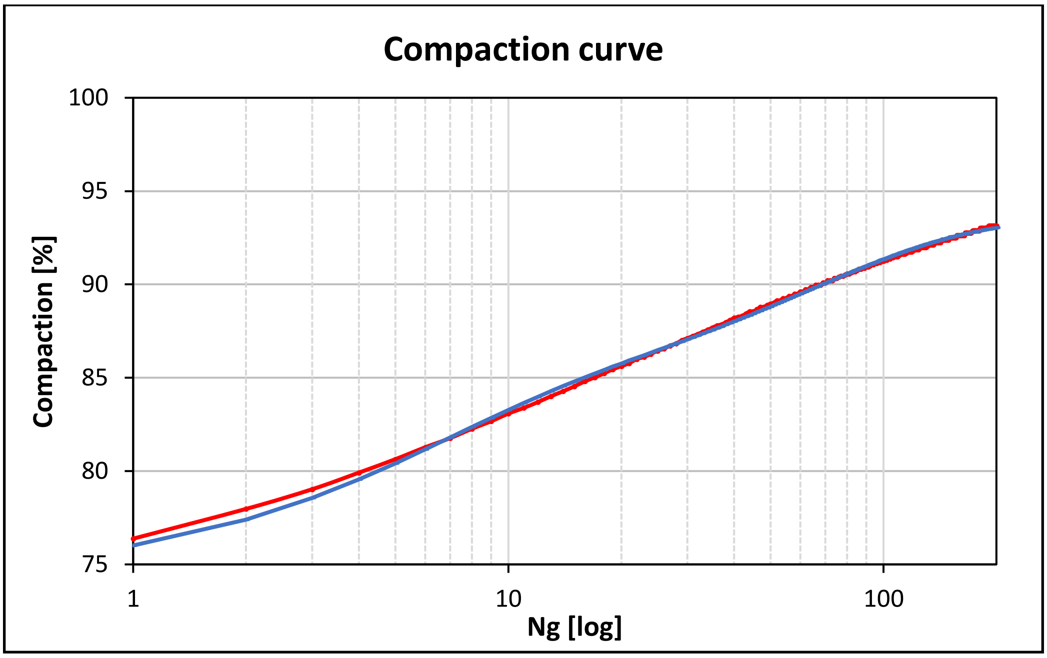

Graph 24: Compaction curve modelled of A/3/160, in semi-logarithmic scale

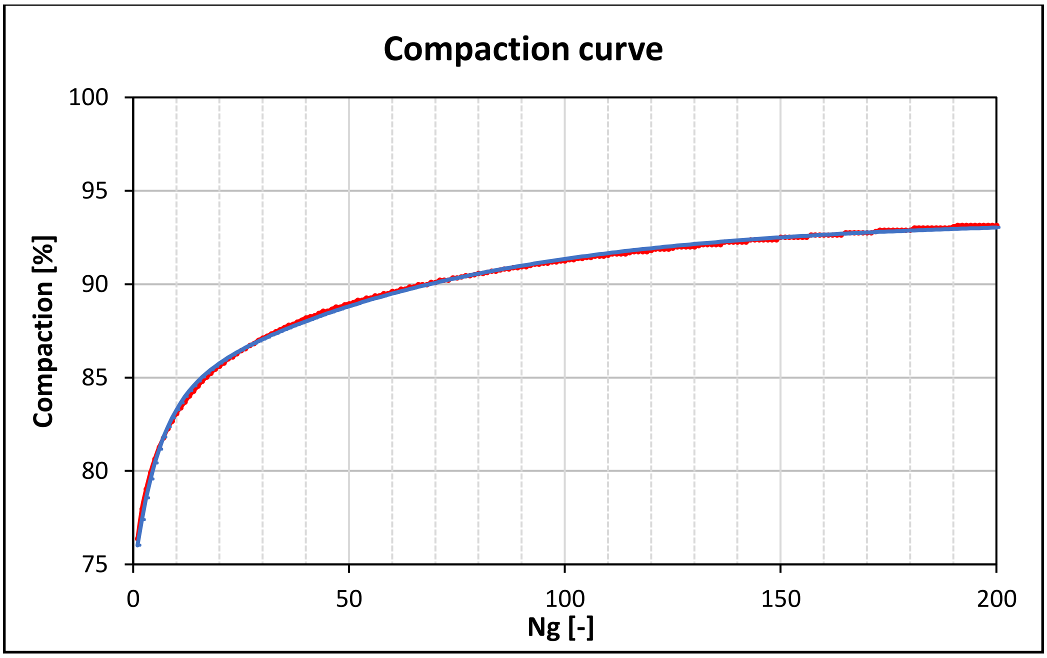

Graph 25: Compaction curve modelled of A/3/160, in normal scale

The parameters of all simulation phase are summarized in the following *Table 31*.

Table 31: Parameters of Spring + 2 Kelvin model curve compaction - at 160 °C

Sample	E_0	E_1	E_2	η_1	η_2	RMS
A/3/160	8.06	58.69	67.80	3729.33	377.04	4.16
A/4.5/160	7.73	53.70	63.95	3505.42	390.02	3.88
B/4.5/160	7.73	52.36	61.00	3160.40	350.11	4.41
A/4.5/X/160	7.69	53.00	65.58	3520.63	387.82	3.86
A/4.5/Y/160	7.71	53.58	62.91	3552.42	386.96	3.80
A/4.5/Z/160	7.71	52.11	66.35	3447.64	412.85	4.12
A/4.9/160	7.72	52.83	63.51	3452.16	397.53	4.11

From a visual result of the simulated curves, it is evident that the selected model can simulate all the compactions curves with good accuracy. Furthermore, all the parameters have stable values comparing with the same stiffness parameters, this is important due to the fact almost all the mixture present similar compaction curve.

The aim of this study was to identify parameters that can highlight different aspects of the compaction phenomenon. To do this, the superposition principle was applied splitting the model compaction curve in three different contribution due to the fact that the used model is a combination of three elements (Spring, Kelvin and Kelvin).

In the following is studied the results of the model's parameters in different condition as the mixtures varying the binder, the mixtures including the additives and the mixture with different skeleton. In this way the objective is to define a correlation between the material and the element of the model.

Variation of the binder dosage

In the following *Table 32* are reported the model's parameters regarding the mixtures with different binder content.

Table 32: Comparison model's parameters varying the binder content

Sample	E_0	E_1	E_2	η_1	η_2	RMS	t_{c1}	t_{c2}
A/3/160	8.06	58.69	67.80	3729.33	377.04	4.16	5.56	63.54
A/4.5/160	7.73	53.70	63.95	3505.42	390.02	3.88	6.10	65.27
A/4.9/160	7.72	52.83	63.51	3452.16	397.53	4.11	6.29	66.00

From the *Table 32* as the binder dosage varies, the contribution of E_0, E_1 and E_2 reflect this aspect in term of final compaction and the time increases to fully develop the compaction.

Furthermore, it is shown in the following graphs the result of the models applying the superposition principle, in order to see better the variation in term of compaction of each element of the model.

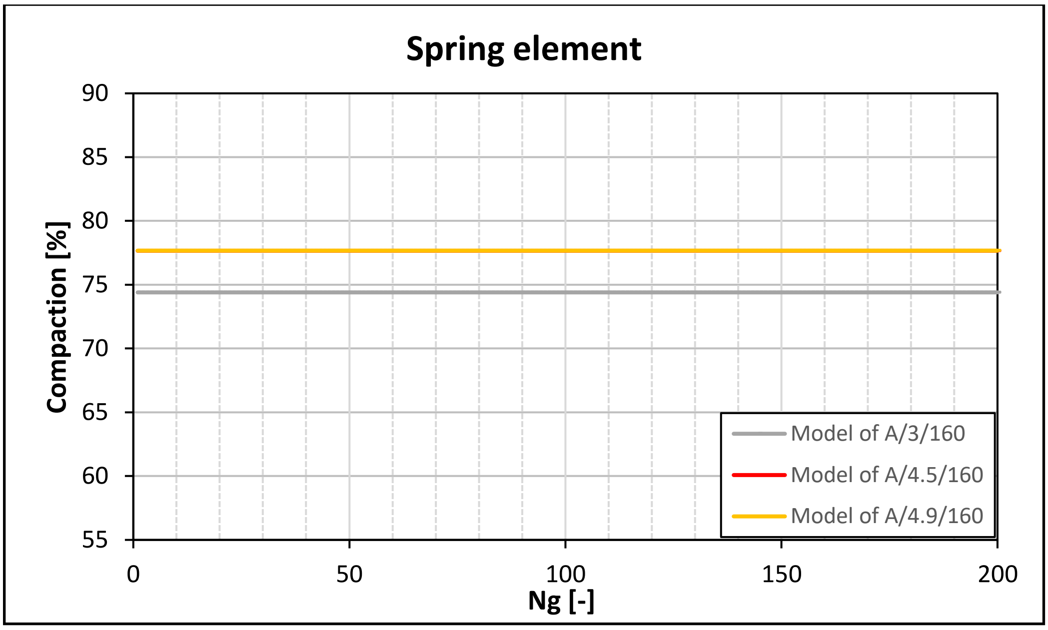

Graph 26: Result of the Spring element varying the binder content at 160 °C

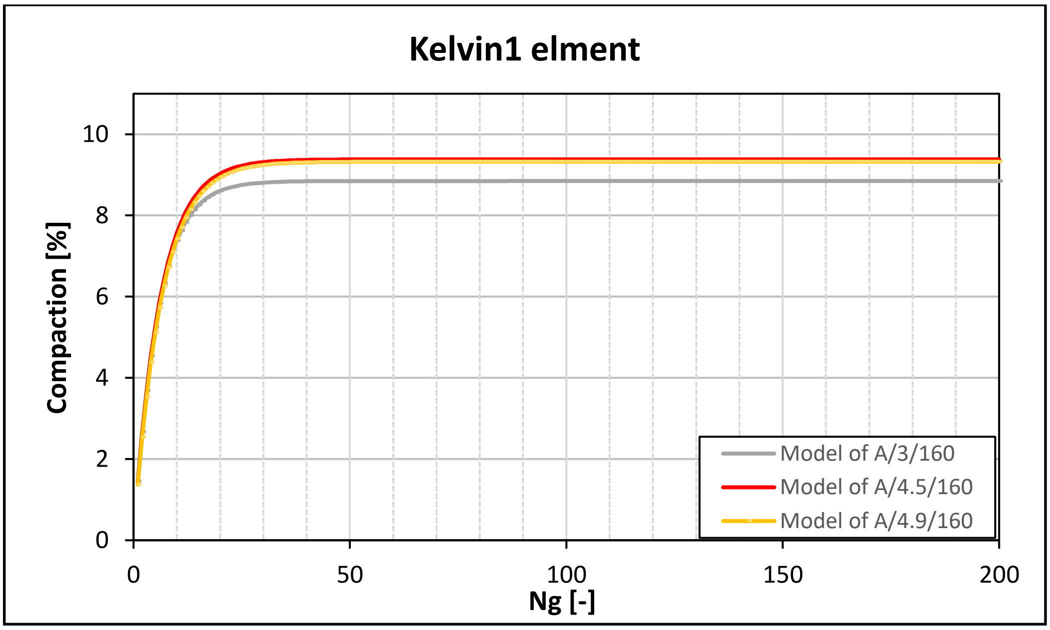

Graph 27: Result of the Kelvin1 element varying the binder content at 160 °C

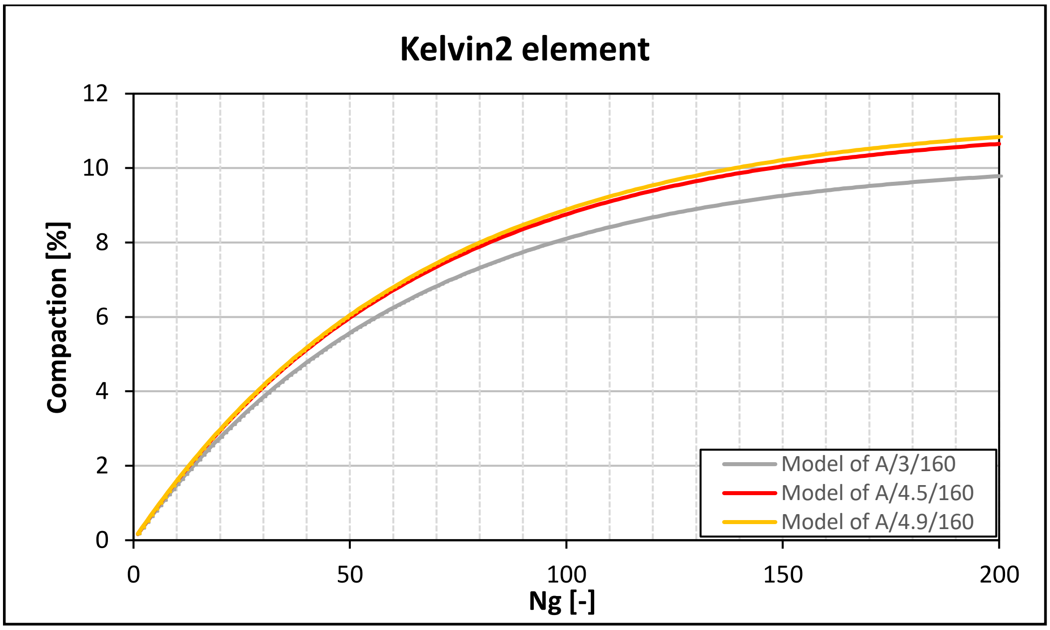

Graph 28: Result of the Kelvin2 element varying the binder content at 160 °C

Using the additives

In the following *Table 33* is shown the result of the model's parameters using the additives compare to the refence one.

Table 33: Comparison model's parameters using the additives

Sample	E_0	E_1	E_2	η_1	η_2	RMS	t_{c1}	t_{c2}
A/4.5/160	7.73	53.70	63.95	3505.42	390.02	3.88	6.10	65.27
A/4.5/X/160	7.69	53.00	65.58	3520.63	387.82	3.86	6.15	66.30
A/4.5/Y/160	7.71	53.58	62.91	3552.42	386.96	3.80	5.91	66.43
A/4.5/Z/160	7.71	52.11	66.35	3447.64	412.85	4.12	6.22	66.17

In this case the mixtures with the presence of additives, the parameters E_0, E_1 and E_2 didn't produce any sensible variation due to the similar compaction by using the gyratory. Regarding the time, the additives slightly act on t_{c2}, increasing it a bit.

In addition, it is shown in the following graphs the result of the models applying the superposition principle, in order to see better the variation in term of compaction of each element of the model.

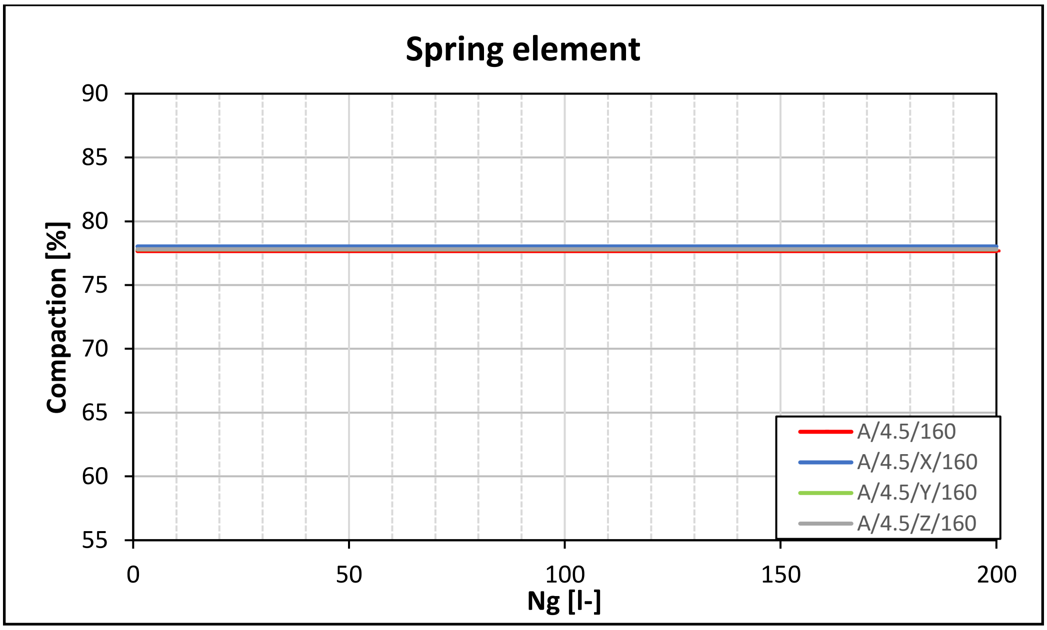

Graph 29: Results of the Spring element using the additives at 160 °C

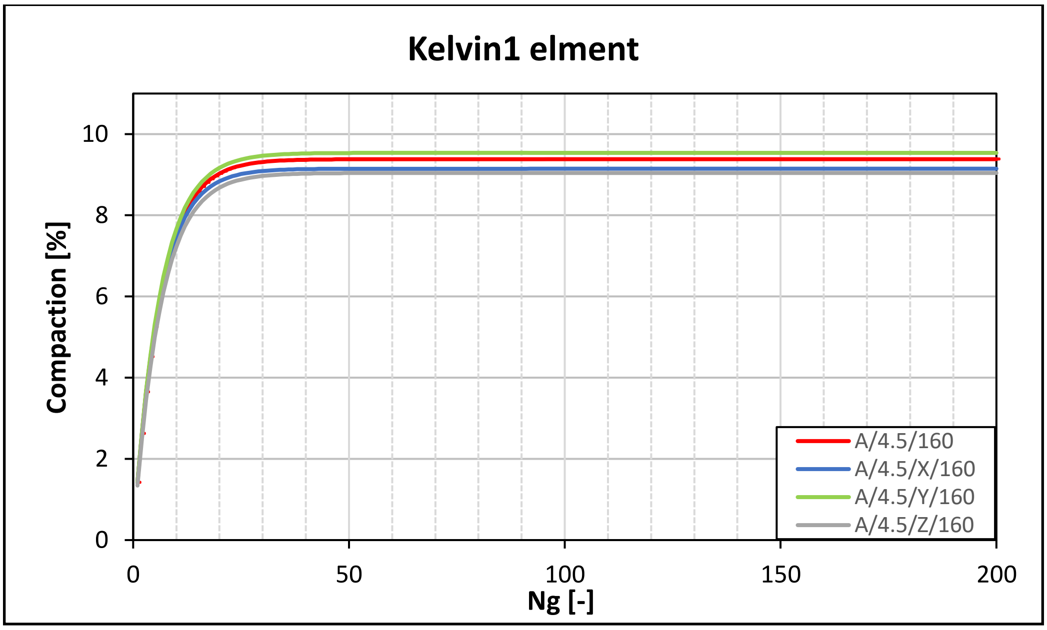

Graph 30: Results of the Kelvin1 element using the additives at 160 °C

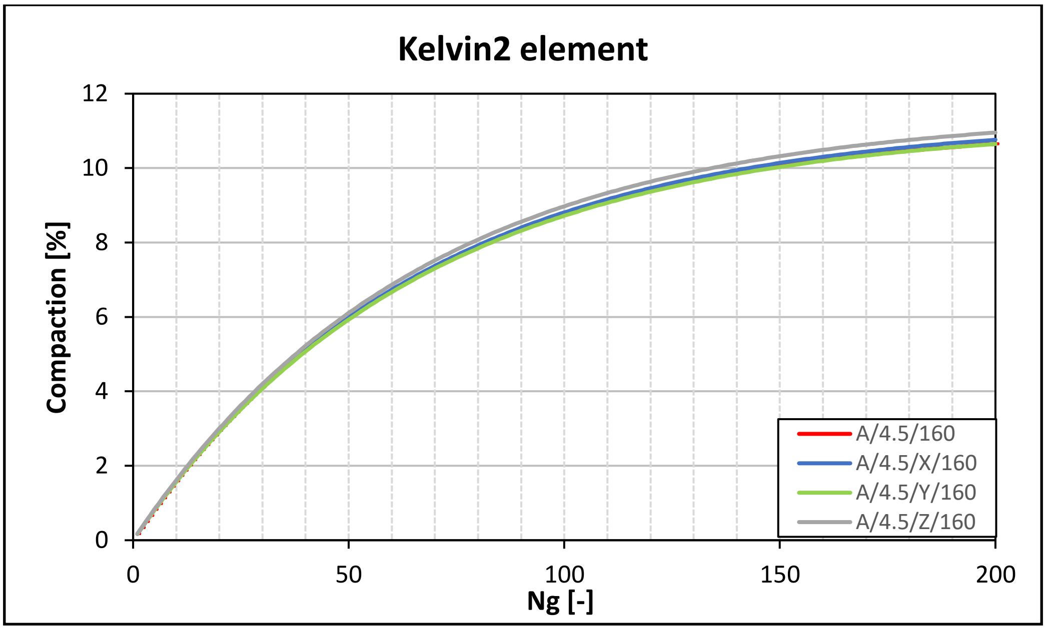

Graph 31: Results of the Kelvin2 element using the additives at 160 °C, in normal scale

Changing the aggregate skeleton

In the next *Table 34* is shown the comparison results of the model's parameters between the reference one and the one with the aggregate skeleton B.

Table 34: Comparison model's parameters changing the skeleton

Sample	E_0	E_1	E_2	η_1	η_2	RMS	t_{c1}	t_{c2}
A/4.5/160	7.73	53.70	63.95	3505.42	390.02	3.88	6.10	65.27
B/4.5/160	7.73	52.36	61.00	3160.40	350.11	4.41	5.74	60.36

In case of changing the granular size distribution with more continuous curve, it fully developed in a lower time reaching higher degree of compaction, the opposite with the varying the binder.

Furthermore, it is shown in the following graphs the result of the models applying the superposition principle, in order to see better the variation in term of compaction of each element of the model.

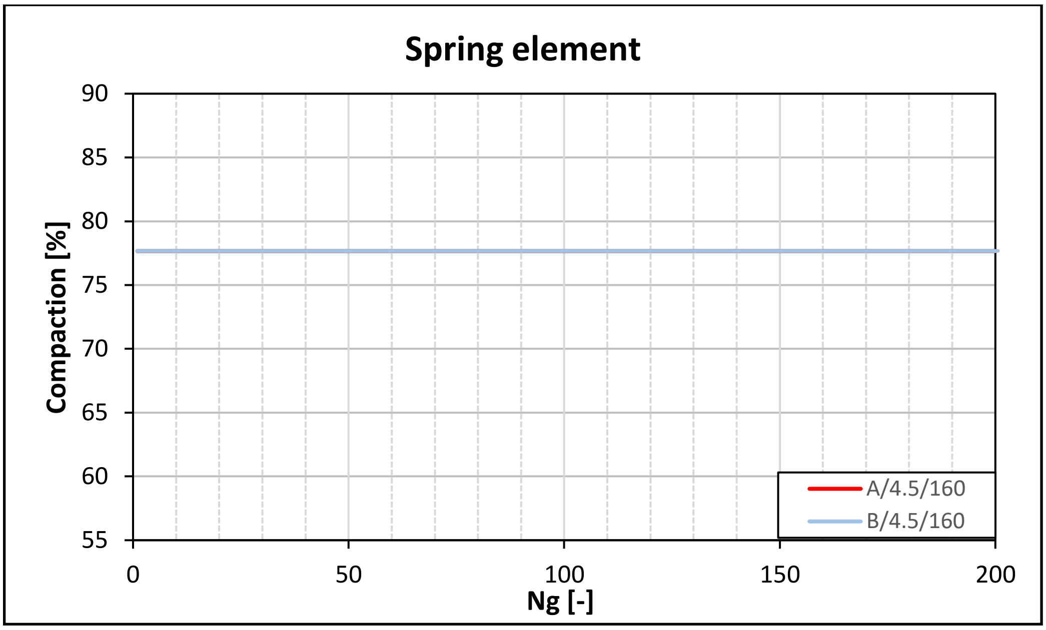

Graph 32: Results of the Spring element changing the aggregate skeleton at 160 °C

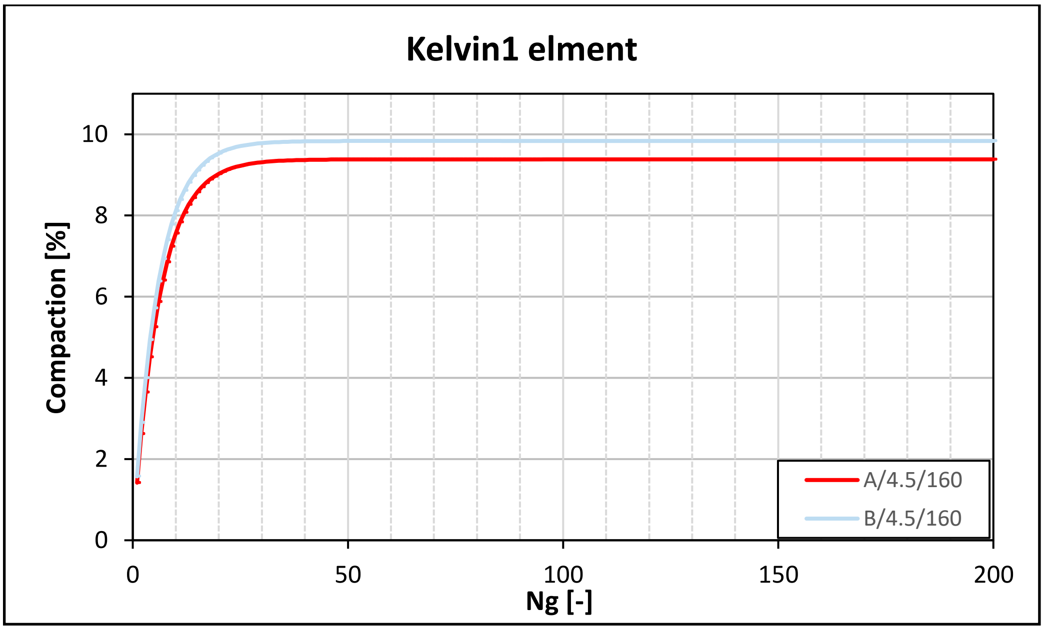

Graph 33: Results of the Kelvin1 element changing the aggregate skeleton at 160 °C

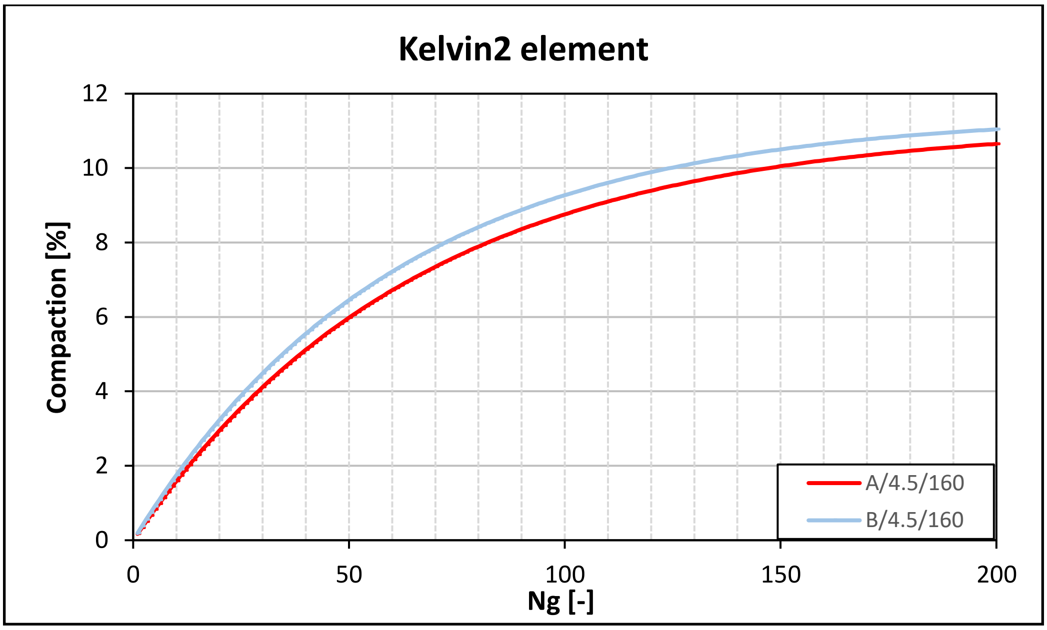

Graph 34: Results of the Kelvin2 element changing the aggregate skeleton at 160 °C

5.4.2 Result of the simulation at different compaction T

In this section is illustrated all the simulation of the mixtures compacted at different temperatures (160 °C, 140 °C and 110 °C). The simulation of compaction at 160 °C are the same to the previous paragraph.

In the followings Tables and Graphs are shown the results.

Table 35: Model's parameters of PMB/Company/4.5%B. at 140 °C

Model	E_0	E_1	E_2	η_1	η_2	RMS
Spring + Kelvin + Kelvin	7.78	54.92	63.94	3466.76	379.54	3.92

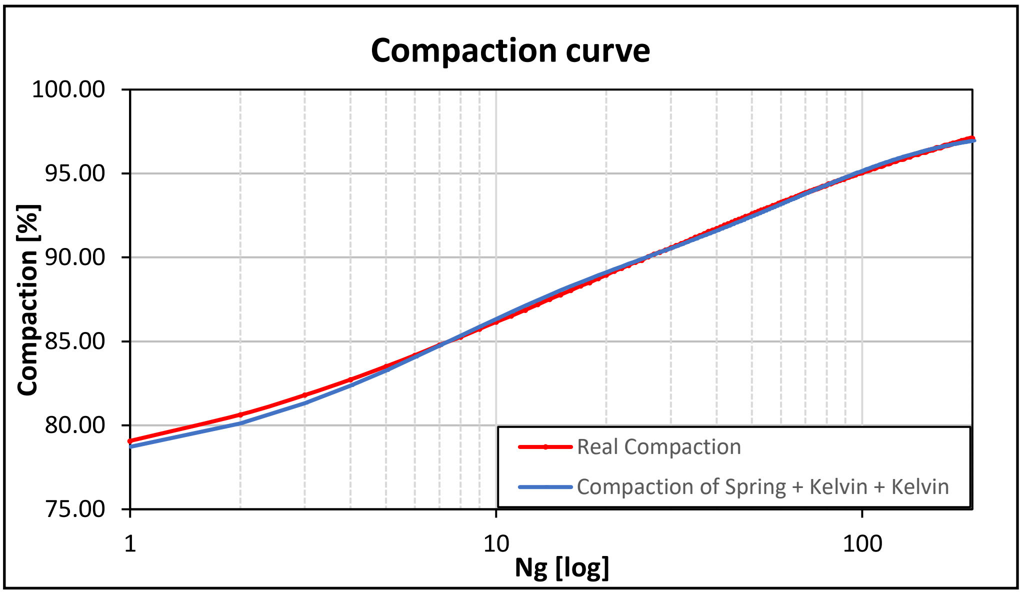

Graph 35: Model compaction curve of A/4.5/140 at 140 °C, in semi-logarithmic scale

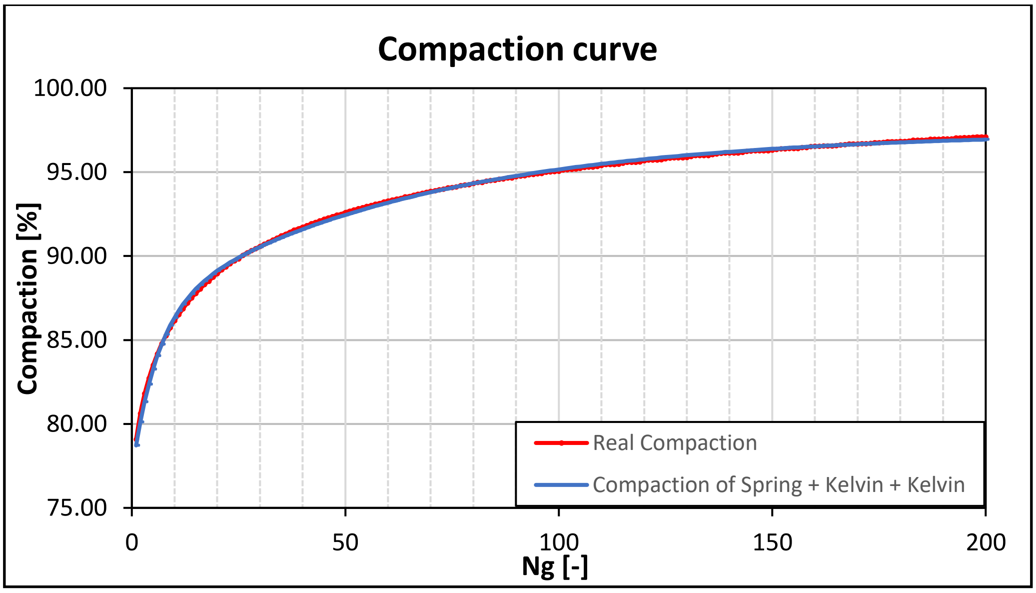

Graph 36: Compaction curve modelled of A/4.5/140 at 140 °C, in normal scale

Table 36: Model's parameters of A/4.5/110 at 110 °C

Model	E_0	E_1	E_2	η_1	η_2	RMS
Spring + Kelvin + Kelvin	7.93	55.14	64.45	3221.93	379.40	4.23

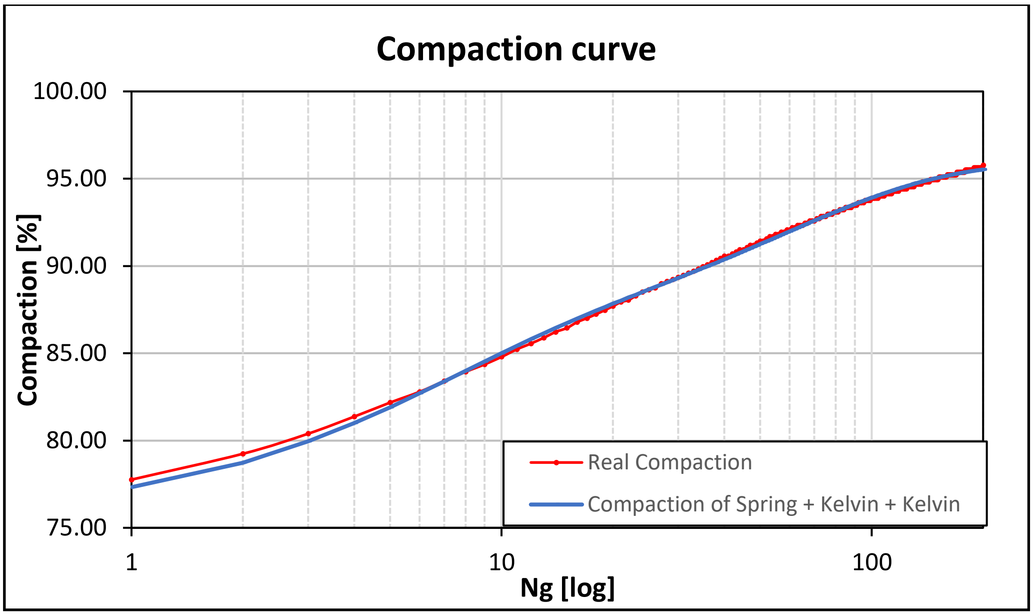

Graph 37: Compaction curve modelled of A/4.5/110 at 110 °C, in semi-logarithmic scale

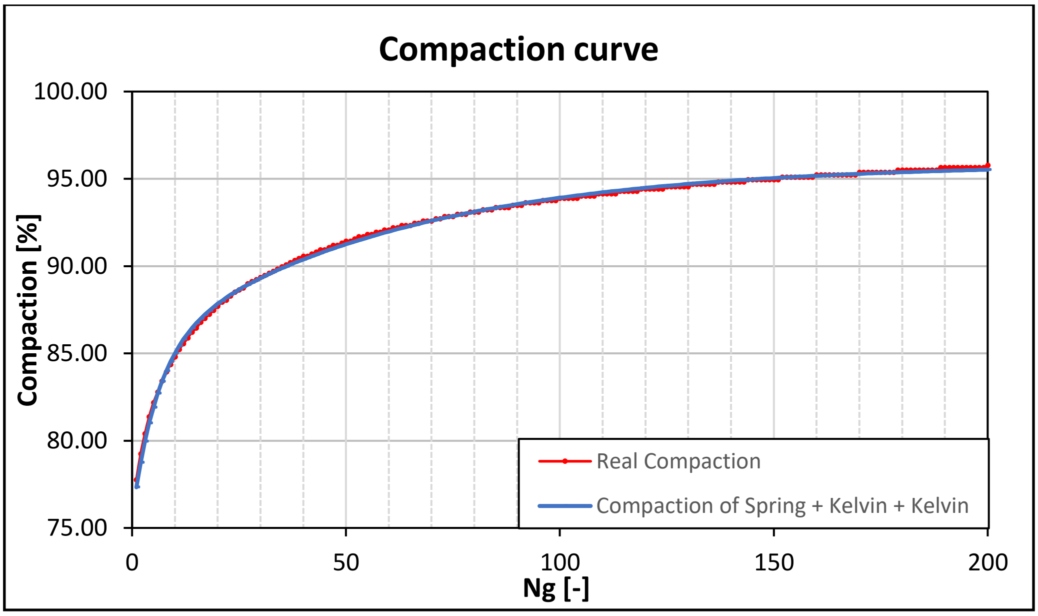

Graph 38: Compaction curve modelled of A/4.5/110 at 110 °C, in normal scale

The parameters of these simulation phase are summarized in the following *Table 39*.

Table 37. Parameters of Spring + 2 Kelvin model curve compaction at different temperatures

Sample	E_0	E_1	E_2	η_1	η_2	RMS	t_{c1}	t_{c2}
A/4.5/160	7.73	53.70	63.95	3505.42	390.02	3.88	6.10	65.27
A/4.5/140	7.78	54.92	63.94	3466.76	379.54	3.92	5.94	63.12
A/4.5/110	7.93	55.14	64.45	3221.93	379.40	4.23	5.89	58.43

In the case of temperature, it increases the compaction by increasing the temperature, by looking the combination of E_0, E_1 and E_2 increase and the time increase too.

In conclusion, it is shown in the following graphs the result of the models applying the superposition principle, in order to see better the variation in term of compaction of each element of the model.

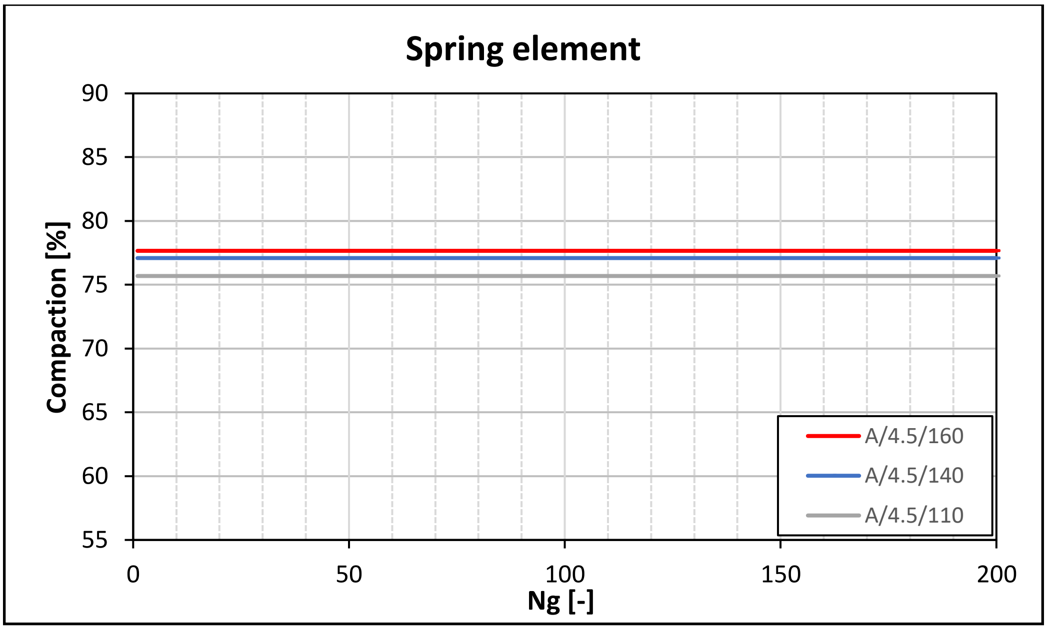

Graph 39:Results of the compaction by the spring element at different temperatures

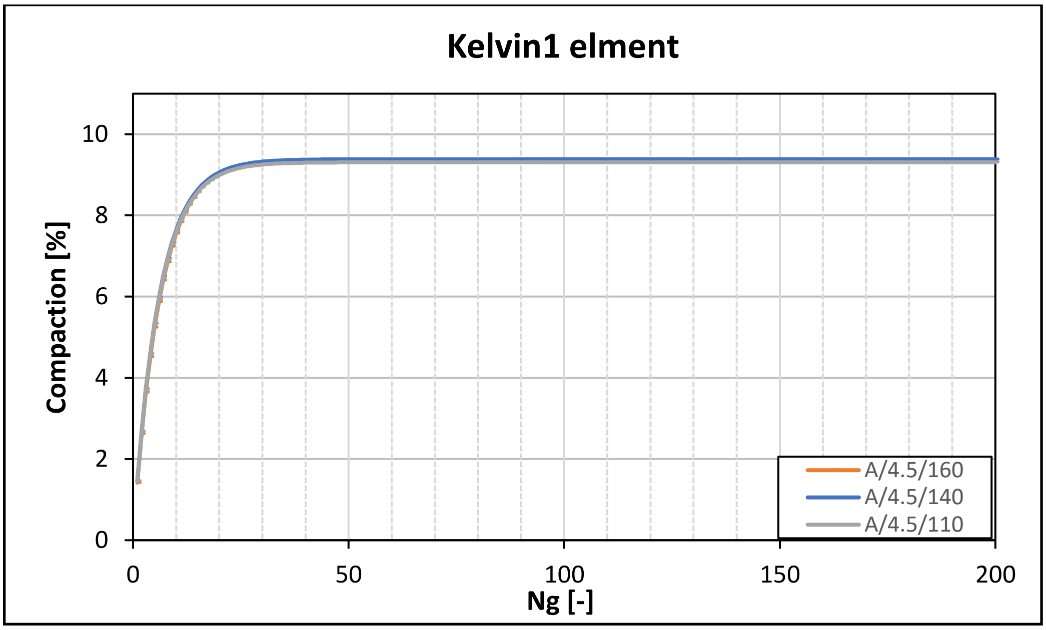

Graph 40: Results of the compaction by the Kelvin1 element at different temperatures,

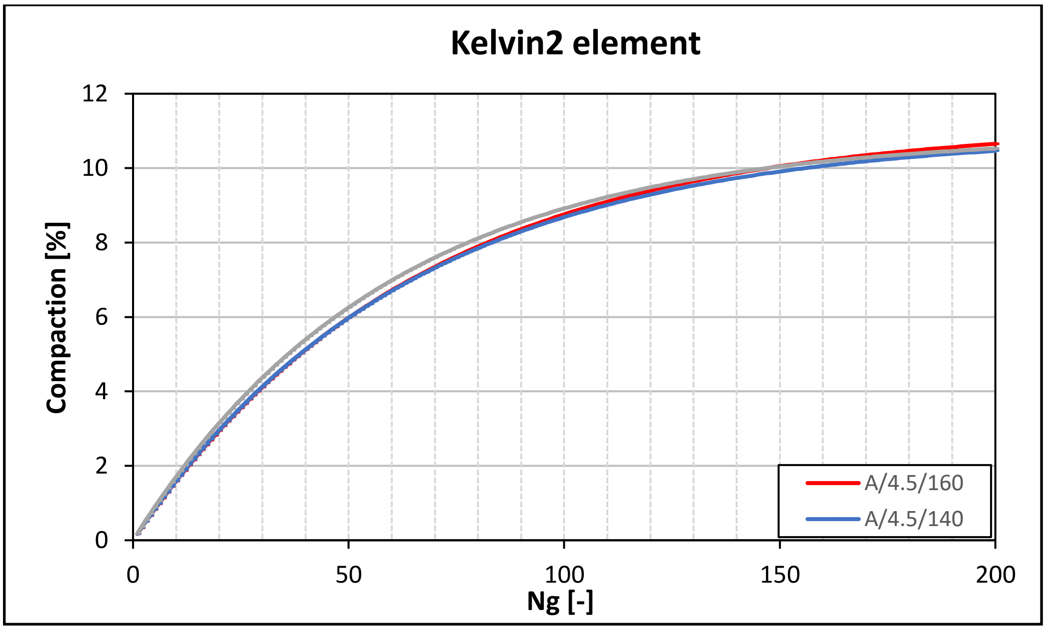

Graph 41: Results of the compaction by the Kelvin2 element at different temperatures,

CHAPTER 6

Conclusions and Future works

6.1 Introduction

In this last chapter the conclusion will complete the study and connect back the statements made.

In this research, six different bituminous mixture were tested using three different additives, varying the binder content, the granular skeleton and the compaction temperature, with the first aim to study the behaviour of the compaction.

The second aim of this study was to develop a mathematical model with the aim to fit the compaction curves obtained in the experimental campaign and from the model's parameters to try to evaluate some quantitative information.

6.2 Conclusion

6.2.1 Compaction process

Generally, most of the mixtures combinations, except one, are characterized by the same granulometric skeleton (A), using the reference granulometric skeleton suggested by the Company.

Regarding the compactions, comparing the bituminous mixture including the additives with the reference one, there was a slight difference in term of compaction. It can be translated that the effect of the additives is not evident during the compaction process by using the GSC.

Instead, the comparison between the reference one and the one with the modified aggregate skeleton (B) having 4.5% of binder content, as expective, it had higher compaction due to the more homogeneous variation of the aggregate size, in this case the reduction of the compaction effort could reach almost the 25%.

From the results of this study, it is observed that the compaction behavior is most depending on the particle size, in particular materials with a more uniform variation of aggregate composition will compact more than uneven material.

After the compaction test, the samples were tested with the ITS test. A remarkable difference was observed in the results of the ITS tests when different additives were used, while, in the case of SGC results, the final compactions were very similar. Comparing the results with the reference mixture (A/4.5/160), the samples including the additives had the 20% of reduction of the ITS value. This happened due to the presence of oil inside the additives that acted like lubricant and reduced the grip between the aggregates. Instead, the samples with the modified aggregate skeleton had an enhancement of the 10% in ITS results due to the higher composition of the aggregates.

6.2.2 Modelling

Three different models were developed in order to simulate the compaction phenomena of the materials. Using the models, the compaction curve of the reference mixture (A/4.5/160) was tested as first, and from the result it was possible to say that the model compose by the Spring and two Kelvin-Voight in series can simulate the compaction curve with an acceptable error. From this consideration the one was selected as the model for develop the compaction curves of all the mixtures performed during the experimental campaign.

From the result of the model, it was possible to see that in some cases, the model's parameters changed significantly compare to the reference one, but in others case only slight differences. In the case of the comparison between the results of the reference one and the one with the modified granulometric skeleton, it was possible to see that the retardation time (t_c) is reducing and increasing the compaction degree. Instead, the comparison with the samples including the additives, it wasn't possible to see some significant variation in the model's parameters.

6.3 Future work

One of the most important further development could be the performance related tests like fatigue or rutting, in order to show the other possible aspects of using additives as the ITS test shown. Another test could be the introduction of in situ test, to study the real compaction behavior of the bituminous mixtures. Perhaps, in this way, it can be possible to see the effect of the additives that the GSC couldn't show.

Regarding the modelling phase, even the model work in all the mixture changing the binder dosage, the use of additives, the aggregate skeleton and the temperature were not evident the definitions of the meaning of the model's elements. It needs greater numbers of data in archived for more various conditions to define the meaning of each parameters. Future works can focus on finding relation between physical phenomenon of compaction in each step and the meaning of the parameters.

BIBLIOGRAPHY

[1] Unknown, «The Constractors,» [Online].

[2] B. E. 12697-8, «Determination of void characteristics of bituminous specimens,» 2018.

[3] C. K. Sridhar Raju, «PERFORMANCE_BASED_MIX_DESIGN_USING_SUPER-PAVE_GYRATORY_COMPACPERFORMANCE-BASED-MIX-DESIGN-USING-SUPER-PAVE-GYRATORY-COMPACTOR-SGC,» september 2003. [Online].

[4] L. A. C. J. a. E. R. B. Jagan M. Gudimettla, «Workability of Hot-Mix Asphalt,» April 2015. [Online].

[5] M. D. Samer Dessouky, «Evaluation of Asphalt Mixes Workability and Compactability Using,» 2015. [Online].

[6] «04 linear viscoelastisity 1 mechanical models,» [Online].

[7] S. M. G. Pullara, «Performance characterization and modelling of cold,» 2018.

[8] J. Lubliner, Plasticity Theory, 2008.

[9] P. Srl, «Rapporto di prova,» 2021.

[10] MAPEI, «Thecnical data sheet ACF-L5,» [Online].

[11] B. E. 933-1, «Tests for geometrical properties of aggregates - Part 1: Determination of particle size distribution - Sieving method,» 2012.

[12] B. E. 932-2, «Tests for general properties of aggregates Methods for reducing laboratory samples,» 1999.

[13] E. B. 1097-6, «TESTS FOR MECHANICAL AND PHYSICAL PROPERTIES OF AGGREGATES - PART 6: DETERMINATION OF PARTICLE DENSITY AND WATER ABSORPTION,» 2013.

[14] B. E. 1097-7, «Tests for mechanical and physical properties of aggregates - Part 7: Determination of the particle density of filler - Pyknometer method,» 2008.

[15] *Capitolato Speciale d'Appalto,* 2020.

[16] K. S. Minhas, «EFFECT OF BINDER CONTENT ON VOLUMETRIC PROPERTIES OF ASPHALT MIXES,» 2019. [Online].

[17] B. E. 12697-35, «laboratory mixing of bituminous materials for the manufacture of specimens,» 2016.

[18] B. E. 12697-5, «test methods for determining the maximum density of a bituminous mixture,» 2018.

[19] B. E. 12697-39, «Bituminous mixtures. Test methods Binder content by ignition,» 2020.

[20] B. E. 12697-31, «Bituminous mixtures. Test methods Specimen preparation by gyratory compactor,» 2019.

[21] B. E. 12607-6, «Bituminous mixtures. Test methods Determination of bulk density of bituminous specimens,» 2020.

[22] B. E. 12697-23, «Bituminous mixtures. Test methods-Determination of the indirect tensile strength of bituminous specimens,» 2017.

[23] «What is it for and how to use the Office Excel Solver,» [Online].